New Trends in the Synthesis of π-Electron Donors for Molecular Conductors and Superconductors

Jun-ichi Yamada* and Hiroki Akutsu

Department of Material Science, Graduate School of Material Science, University of Hyogo, 3-2-1 Kouto, Kamigori-cho, Ako-gun, Hyogo 678-1297, Japan

Hiroyuki Nishikawa and Koichi Kikuchi

Department of Chemistry, Graduate School of Science, Tokyo Metropolitan University, Hachioji, Tokyo 192-0397, Japan

Received February 20, 2004

Contents

1. Introduction

Research on the development of new molecular-based organic metals and superconductors was stimulated by the first finding of metallic conductivity in a charge-transfer (CT) complex composed of tetrathiafulvalene (TTF, Figure 1) and tetracyanoquinodimethane (TCNQ)[1] and was subsequently accelerated by the discovery of superconductivity in the CT salts of tetramethyltetraselenafulvalene (TMTSF) followed by that in the CT salts of bis(ethylenedithio)-tetrathiafulvalene (BEDT-TTF or ET).[2] Simultaneously, continuous interest in this field has been sustained by synthetic organic chemists, resulting in the production of a huge number of π-electron donors for molecular conductors.[3] The ordinary molecular design of π-donors has evolved mainly from (i) the planarity for a facile formation of donor stacking, (ii) the extension of π-conjugation for a decrease in the on-site Coulombic repulsion involved in the formation of a dicationic species [an increase in delocalization of the generating positive charge(s)], and (iii) the introduction of chalcogen atoms for an increase in dimensionality of the conduction pathway, which was illustrated by the structural characteristics of the ET-based superconductors with nearly isotropic conductivity in the donor sheet including the intermolecular S···S network [two-dimensional (2D) character]. On the contrary, our molecular design strategy for constructing new π-donors is based on the following requirements: (i) extension of the σ-bond framework, which will lead to the lack of planarity, and (ii) reduction of the π-electron system, which will increase the on-site Coulombic repulsion. The motivation in this strategy is to give relief to the tight intermolecular cohesion leading to the stable metallic state so that a synthetic avenue to the realization of organic superconductivity might be opened up, as suggested by a series of studies of the phase diagrams

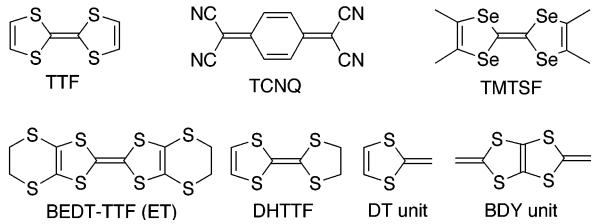

Figure 1.

* To whom correspondence should be addressed. Phone: +81(0)791-58-0162. Fax: +81(0)791-58-0164. E-mail: yamada@sci.u-hyogo.ac.jp.

10.1021/cr0306687 CCC: $48.50
Published on Web 09/08/2004

Jun-ichi Yamada obtained his B.Sc. (1982) and M.Sc. (1984) degrees from Tohoku University. In 1986 he started his academic career as a Research Associate at the same university, where he studied new synthetic methods using organometallics. In 1988 he received his Ph.D. degree from Tohoku University under the supervision of Professor Yoshinori Yamamoto. In 1990 he moved to Himeji Institute of Technology, the predecessor of the present University of Hyogo, to join the group of Professor Hiroyuki Anzai and then was promoted to Associate Professor. He received the Chemical Society of Japan Award for Young Chemists in 1992. His current research interests embrace the development of new synthetic methodology and the design and synthesis of new organic materials with unconventional electrical and magnetic properties.

Hiroki Akutsu received his Ph.D. degree from Tokyo University of Science in 1996 under the supervision of Professor Tokiko Uchida. He was an IMS Research Fellow (1996–1998) in Professor Hayao Kobayashi's group and a postdoctoral fellow (1998–1999) with Professors Michio Sorai and Kazuya Saito in Osaka University. In 1999 he joined the group of Professors Shin′ichi Nakatsuji and Jun-ichi Yamada as a Research Associate. He studied at Professor Peter Day's group in DFRL in the Royal Institution from 2001 to 2002. His research interests focus on the structural, electrical, and magnetic properties of molecular-based conductors and magnets.

Hiroyuki Nishiakwa graduated from Kyoto University in 1988 and received his Ph.D. degree in 1993 for his studies on new organic conductors under the guidance of Professor Tokio Yamabe. He worked as a postdoctoral fellow with Professor Klaus Bechgaard at Risø National Laboratory in Denmark from 1993 to 1994. Then he joined the group of Professor Isao Ikemoto at Tokyo Metropolitan University as a Research Associate (1994–2004). He moved to the University of Tsukuba as an Associate Professor to join the group of Professor Hiroki Oshio in 2004. His current interests cover the development of new organic conductors, new donor–acceptor systems for photoactive materials, and new molecular coordination compounds with electrical and magnetic properties.

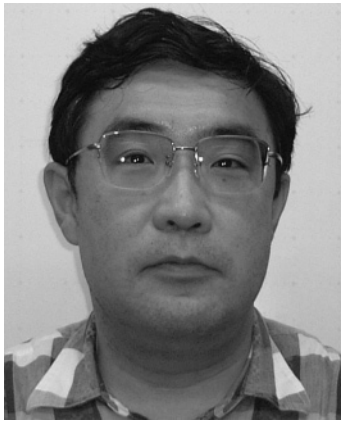

Koichi Kikuchi obtained his B.Sc. (1980) and Ph.D. (1985) degrees from the University of Tokyo. In 1985 he started his academic career as a Research Associate at Tokyo Metropolitan University and was promoted to Associate Professor in 1993. His current research lies in the fields of metallofullerenes and chiral molecular magnets as well as molecular superconductors.

of TMTSF[4] and ET[5] superconductors that the superconducting state lies immediately adjacent to the antiferromagnetic insulating state. Therefore, if π-donors being adequately designed according to the above requirements could produce superconductors, the way of thinking of synthetic chemists for the design of new organic superconductors would change. The emphasis of this review is thus mainly on our recent studies to explore organic metals and superconductors.[6] Our efforts will be described in four parts: (1) studies on the development of new synthetic methods, (2) studies of TTF donors with extended σ-bond framework, (3) studies of dihydroTTF (DHTTF) donors and their analogues, each π-system of which comprises only one 1,3-dithiol-2-ylidene (DT) unit, and (4) studies of a new donor family that contains the bis-fused DT (BDY) unit as a common π-system. The definition of abbreviations used herein for naming donor molecules is summarized in Table 1.

2. Lewis-Acid-Promoted Reactions

TTF derivatives serve as donor components of molecular conductors, so that extensive studies on chemical modifications of the TTF skeleton have been made to develop new molecular conductors with metallic conductivity and superconductivity.[3b−g] These studies result, for example, in heteroatom-substituted, halogenated, stable radical-substituted, dimeric (directly linked, spacer-incorporated, cyclophane-type, or fused), and oligomeric (linear or macrocyclic)

Table 1. Abbreviations of Donor Molecules

MDT-TTF	methylenedithiotetrathiafulvalene
DMET	dimethyl(ethylenedithio)diselenadithiafulvalene
TMET-STF	trimethylene(ethylenedithio)diselenadithiafulvalene
MDHT	methylenedithio(dihydro)tetrathiafulvalene
EDHT	ethylenedithio(dihydro)tetrathiafulvalene
EDHS	ethylenedithio(dihydro)diselenadithiafulvalene
EDDT	2-(4,5-ethylenedithio-1,3-dithiol-2-ylidene)-1,3-dithiane
EDDH-TTP	2-(4,5-ethylenedithio-1,3-dithiol-2-ylidene)-5-(1,3-dithiolan-2-ylidene)-1,3,4,6-tetrathiapentalene
EDOT-TTP	2-(4,5-ethylenedithio-1,3-dithiol-2-ylidene)-5-(1,3-oxathiolan-2-ylidene)-1,3,4,6-tetrathiapentalene
EDDT-TTP	2-(4,5-ethylenedithio-1,3-dithiol-2-ylidene)-5-(1,3-dithian-2-ylidene)-1,3,4,6-tetrathiapentalene
DTDH-TTP	2-(1,3-dithiol-2-ylidene)-5-(1,3-dithiolan-2-ylidene)-1,3,4,6-tetrathiapentalene
DMtTSF	dimethyl(trimethylene)tetraselenafulvelene
DOET	(1,4-dioxane-2,3-diyldithio)ethylenedithiotetrathiafulvalene
DOES	(1,4-dioxane-2,3-diyldithio)ethylenediselenotetrathiafulvalene
DOEO	(1,4-dioxane-2,3-diyldithio)ethylenedioxotetrathiafulvalene
DOT	(1,4-dioxane-2,3-diyldithio)tetrathiafulvalene
DTET	(1,4-dithiane-2,3-diyldithio)ethylenedithiotetrathiafulvalene
DHDIET	(5,6-dihydro-1,4-dithiin-2,3-diyldithio)ethylenedithiotetrathiafulvalene
DO-MET	(1,3-dioxolan-2-yl)methylenedithio(ethylenedithio)tetrathiafulvalene
DO-MMT	(1,3-dioxolan-2-yl)methylenedithio(methylenedithio)tetrathiafulvalene
DT-MET	(1,3-dithiolan-2-yl)methylenedithio(ethylenedithio)tetrathiafulvalene
OT-MET	(1,3-oxathiolan-2-yl)methylenedithio(ethylenedithio)tetrathiafulvalene
DOA-MET	(1,3-dioxan-2-yl)methylenedithio(ethylenedithio)tetrathiafulvalene
DTA-MET	(1,3-dithian-2-yl)methylenedithio(ethylenedithio)tetrathiafulvalene
Me-MET	methylmethylenedithio(ethylenedithio)tetrathiafulvalene
Et-MET	ethylmethylenedithio(ethylenedithio)tetrathiafulvalene
Me-MDHT	methylmethylenedithio(dihydro)tetrathiafulvalene
Et-MDHT	ethylmethylenedithio(dihydro)tetrathiafulvalene
BDDT-TTF	bis(1,4-dioxane-2,3-diyldithio)tetrathiafulvalene
BDTET	bis(1,4-dithiane-2,3-diyldithio)tetrathiafulvalene
TOET	bis(1,4-oxathiane-2,3-diyldithio)tetrathiafulvalene
MET	methylenedithio(ethylenedithio)tetrathiafulvalene
DODHT	(1,4-dioxane-2,3-diyldithio)dihydrotetrathiafulvalene
BDT-TTP	2,5-bis(1,3-dithiol-2-ylidene)-1,3,4,6-tetrathiapentalene
DTEDT	2-(1,3-dithiol-2-ylidene)-5-[2-(1,3-dithiol-2-ylidene)ethylidene]-1,3,4,6-tetrathiapentalene
BDH-TTP	2,5-bis(1,3-dithiolan-2-ylidene)-1,3,4,6-tetrathiapentalene
BDA-TTP	2,5-bis(1,3-dithian-2-ylidene)-1,3,4,6-tetrathiapentalene
DHDA-TTP	2-(1,3-dithiolan-2-ylidene)-5-(1,3-dithian-2-ylidene)-1,3,4,6-tetrathiapentalene
DHDE-TTP	2-(1,3-dithiolan-2-ylidene)-5-(1,3-dithiepan-2-ylidene)-1,3,4,6-tetrathiapentalene

TTFs.[7] With such modifications, development of a new methodology for the efficient synthesis of the desired TTF-type donor systems has been the major focus of synthetic chemists. From a synthetic point of view, the coupling reaction between 1,3-dichalcogenole-2-chalcogenones using trialkyl phosphite, e.g., $(MeO)_3P$ or $(EtO)_3P$, is a most powerful tool for constructing not only tetrachalcogenafulvalene (TCF) derivatives but also π-electron donors containing 1,3-dichalcogenol-2-ylidene moieties. In addition, useful methods for the preparation of a variety of 1,3-dichalcogenole-2-chalcogenones have been reviewed by Becher et al. (the cyanoethyl protection/deprotection protocol)[8] and Takimiya et al. (the one-pot method).[9] However, application of the $(RO)_3P$-mediated coupling reaction to the synthesis of unsymmetrical TCF derivatives encounters, in principle, the concomitant formation of two symmetrical byproducts (Scheme 1), and the separation of the desired unsymmetrical derivative from the resulting mixture frequently meets with difficulties. Therefore, an alternative methodology is required for the exclusive formation of unsymmetrical derivatives. Furthermore, to construct TTF donors with extended σ-bond framework (vide infra, sections 2.2 and 2.3), it was desirable to develop new synthetic methods for the preparation of their building blocks.

We found that the use of Lewis-acid-promoted reactions allows the settlement of the above-mentioned issues. The following three sections will describe the Me_3Al-promoted reaction to form a 1,3-dichalcogenol-2-ylidene moiety, the BF_3-promoted reaction to prepare 1,3-dithiole-2-chalcogenones extended by a heterocycle, and the Lewis-acid-promoted alkylation of 1,3-dithiole-2-chalcogenones, respectively.

Scheme 1

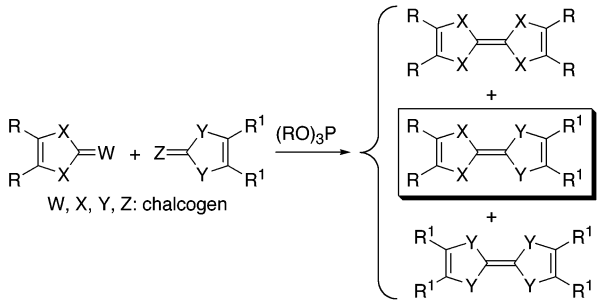

2.1. Me_3Al-Promoted Reaction

In addition to the Wittig- or Wittig−Horner-type condensation, the Me_3Al-promoted coupling reaction of organotin compounds with esters (Scheme 2)[10] is recognized as a versatile non-phosphite methodology for constructing unsymmetrical TTFs, including diselenadithiafulvalenes (DSDTFs), without the forma-

Scheme 2

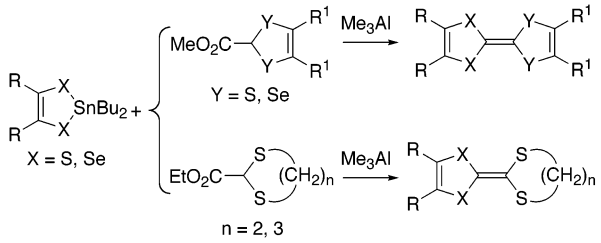

tion of symmetrical byproducts.[9b,11] For example, this coupling reaction allowed the construction of MDT-TTF,[12] DMET,[13] and TMET-STF (Figure 2),[14] which

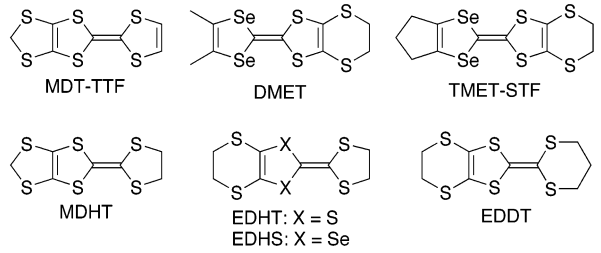

Figure 2.

have given rise to superconducting salts. Additionally, application of this coupling reaction to the synthesis of DHTTFs and their selenium and dithiane analogues, such as MDHT, EDHT, EDHS, and EDDT (Figure 2), has been accomplished. The organotin dithiolates and diselenolates essential to the reaction are easily accessible from the corresponding 1,3-dithiol- and 1,3-diselenol-2-ones via reaction with MeMgBr in THF or NaOMe in MeOH followed by trapping with Cl_2SnBu_2 (Scheme 3).[6a] As for the

Scheme 3

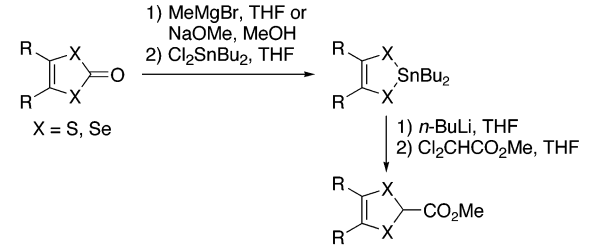

desired ester partners, they can be prepared by transmetalation of the corresponding organotin compounds with 2 equiv of *n*-BuLi and subsequent treatment with methyl dichloroacetate (Scheme 3).[6a] Another useful application of this coupling reaction can be found in the short-step synthesis of various TTF-fused donor systems. For instance, Scheme 4 shows the synthetic route to the fused TTF-DSDTF donor **6**.[10c] Basic cleavage of thiapendione **1** with NaOMe followed by trapping with Cl_2SnBu_2 gave tin dithiolate **2** (96% yield), which reacted with ester **3** in the presence of Me_3Al to furnish DSDTF derivative **4** with a fused 1,3-dithiol-2-one ring (33% yield) as a precursor of **6**. The final product **6** was obtained by the $(MeO)_3P$-mediated reaction of **4** with thione **5** in 46% yield. In a similar manner, preparation of precursors **7a**−**c** (Figure 3) for other TTF-fused donor systems was effected by the Me_3Al-promoted reaction

Scheme 4

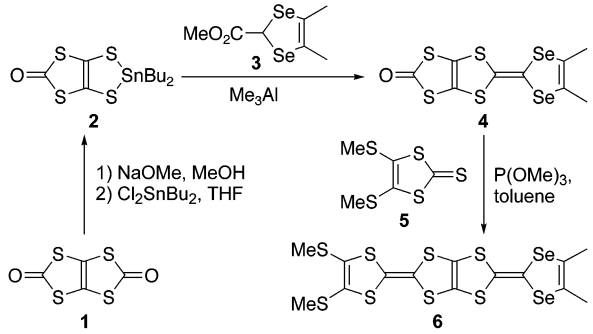

of **2** with the corresponding esters (**7a**, 48% yield; **7b**, 37% yield; **7c**, 23% yield). Subsequent cross-coupling of **7a**−**c** and thione **8a** using $(MeO)_3P$ gave the ethylenedithio-substituted TTF-DHTTF donor EDDH-TTP and its oxygen and dithiane analogues EDOT-TTP and EDDT-TTP in 80%, 62%, and 30% yields, respectively. For synthesis of the parent TTF-DHTTF donor DTDH-TTP, demethoxycarbonylation of **9**, prepared by the $(MeO)_3P$-mediated coupling of **7a** and thione **8b** in 82% yield, by using $LiBr\cdot H_2O$ in HMPA was employed (40% yield).[15]

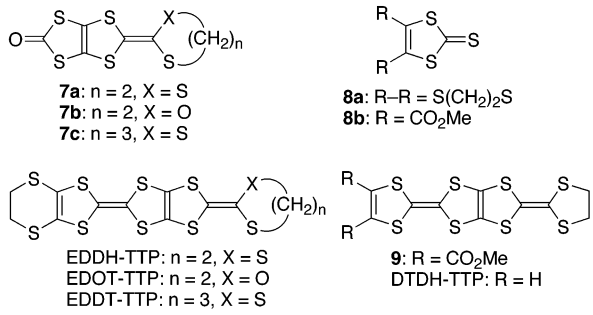

Figure 3.

The yield of the product in the Me_3Al-promoted reaction is sometimes improved by alternating the order of addition in the experiment,[10c] i.e., a tin dichalcogenolate is first reacted with Me_3Al, and then an ester is added. In this case, it is likely that the Sn/Al transmetalation occurs and the resulting bis(dimethylaluminum) dichalcogenolate reacts with the ester.[11a] In the synthesis of the selenium analogues of DHTTFs, e.g., EDHS (Figure 2), it was found that the reaction of tin diselenolates is relatively slow in comparison with that of tin dithiolates.[10a,c] To clarify the applicability of the Me_3Al-promoted coupling reaction in tetraselenafulvalene (TSF) synthesis, we sought to construct DMtTSF (Scheme 5)[6a] because

Scheme 5

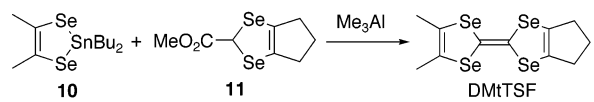

purification of DMtTSF obtained by the $(MeO)_3P$-mediated cross-coupling has been reported to require tedious procedures.[16] Treatment of tin diselenolate **10** with Me_3Al followed by addition of ester **11** provided the pure DMtTSF donor, but its yield was only 3%. Our attempts to improve this low yield by

varying the reaction conditions or use of other Lewis acids met with futility.

2.2. BF_3-Promoted Reaction

Our next search for the synthetic possibilities presented by the combination of organotin compounds and a Lewis acid involved the BF_3-promoted reaction of tin dithiolates with 2,3-dihalo-1,4-dichalcogenane.[17] As shown in Scheme 6, tin dithiolate **2**

Scheme 6

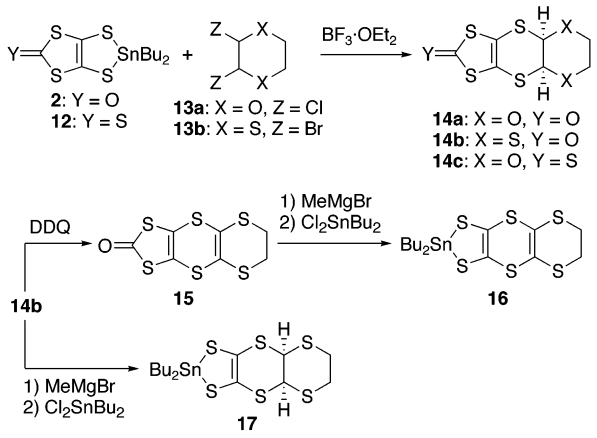

reacted smoothly with dihalides **13a**,**b** in the presence of $BF_3{\cdot}OEt_2$ (2 equiv) to give the dioxane- and dithiane-fused oxones **14a**,**b** in 91% and 68% yields, respectively. Likewise, the dioxane-fused thione **14c** was obtained by the $BF_3{\cdot}OEt_2$ (2 equiv) promoted reaction of **12** with **13a** in 63% yield. It has been reported that **14c** can be prepared by [4 + 2] cycloaddition of oligo(1,3-dithiole-2,4,5-trithione) to 1,4-dioxene,[18] whereas there had been no report on the preparation of **14b**. The cis stereochemistry for the fusion pattern of the dichalcogenane ring in **14a** or **14b** was secured by X-ray crystallographic analysis.[15] Oxidation of the tetrathioethane moiety of **14b** was carried out by reaction with DDQ, affording the dihydrodithiin-fused oxone **15** in 60% yield. Oxones **14b** and **15** could be converted into tin dithiolates **16** and **17**. Oxones **14a**,**b** and tin dithiolates **16** and **17** were used for the $(RO)_3P$-mediated and Me_3Al-promoted coupling reactions, respectively, leading to a series of the heterocycle-fused TTF donors, several of which are shown in Figure 4.[17,19]

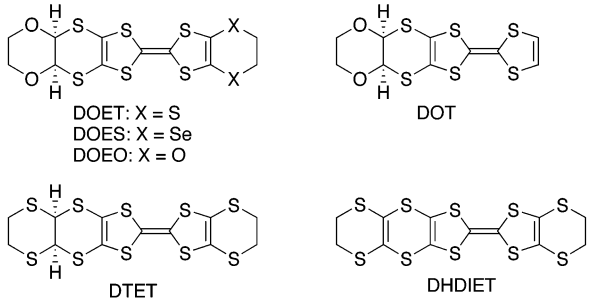

Figure 4.

On the other hand, as shown in Scheme 7, reaction of the dioxane-fused tin dithiolate **18**, derived from **14a**, with ester **19** with the aid of Me_3Al gave a novel

Scheme 7

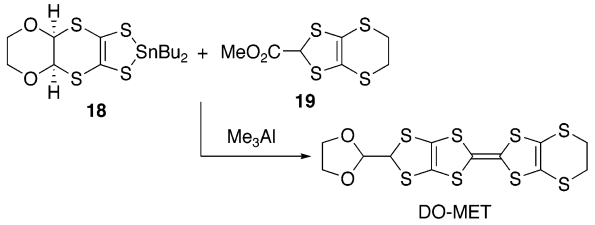

TTF donor linking a dioxolane ring via a σ-bond (DO-MET, 16% yield).[20] This reaction involves the skeletal rearrangement of the bis-fused six-membered ring to the five-membered biheterocycle. To improve the yield of DO-MET and also to construct analogous heterocycle-linked TTF donors, we investigated an efficient preparation of their building blocks.[21] On treatment with an excess of $BF_3{\cdot}OEt_2$ (10 equiv), the dioxane-fused oxone **14a** underwent isomerization to give the dioxolane-attached oxone **20a** (Figure 5)

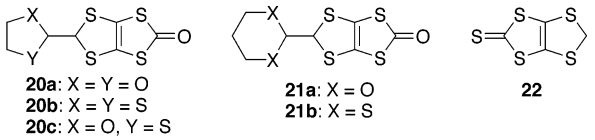

Figure 5.

together with a trace amount of the recovered **14a** (80% yield, **20a**:**14a** = 46:1 by ^1H NMR). Purification of **20a** could be conducted by recrystallization. Scheme 8 shows a postulated mechanism for the isomeriza-

Scheme 8

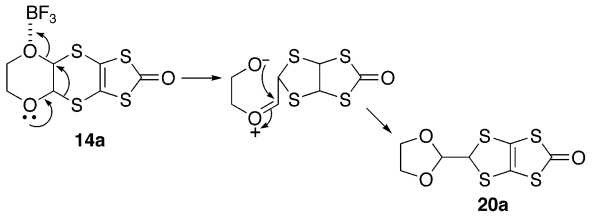

tion.[21b] Furthermore, the addition of 1,2-ethanedithiol in the isomerization reaction of **14a** gave the dithiolane-attached oxone **20b** in 95% yield. The formation of **20b** is thought to involve isomerization of **14a** to **20a** followed by dithioacetalization of **20a**; however, an alternative pathway via cleavage of the *O*,*S*-acetal of **14a** by nucleophilic attack of the sulfur atom of 1,2-ethandithiol (Scheme 9) is also undeniable.[21b] Oxathioacetalization of **20a** with

Scheme 9

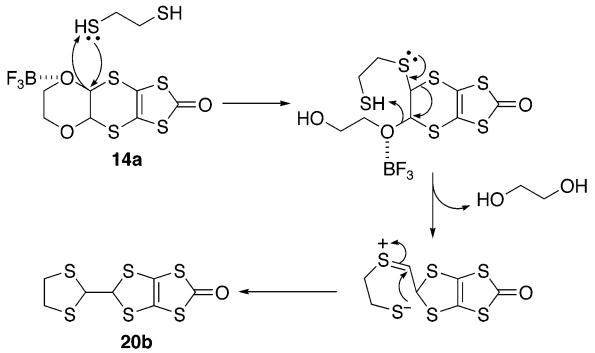

2-mercaptoethanol in the presence of 10 equiv of $BF_3{\cdot}OEt_2$ gave oxone **20c** in 40% yield. Similar to the preparation of **20b**, the $BF_3{\cdot}OEt_2$ (10−13 equiv) promoted reaction of **14a** with 1,3-propanediol and 1,3-propanedithiol furnished the dioxane- and dithiane-attached oxones **21a**,**b** in 59% and 70% yields, respectively.[22] By the $(MeO)_3P$-mediated cross-coupling with thione **8a** (Figure 3) or **22**, oxones **20a**−**c** and **21a**,**b** were converted into DO-MET (80% yield) and related TTF donors, such as DO-MMT (Figure 6, 58% yield), DT-MET (94% yield), OT-MET (83% yield), DOA-MET (89% yield), and DTA-MET (81% yield).

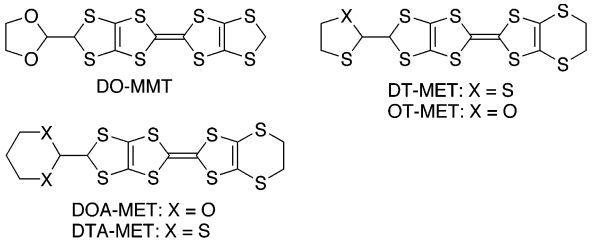

Figure 6.

2.3. Monoalkylation of 1,3-Dithiole-2-chalcogenones

Other than a heterocycle, an attractive σ-bond framework for extending TTF donors is a simple alkyl group. However, introduction of an alkyl substituent into the periphery of TTF donors occasionally results in generation of a chiral carbon center.[23] Thus, considering the molecular symmetry to avoid the chirality problem, the achiral 4,5-(alkylmethylenedithio)-1,3-dithiole-2-chalcogenones **23** and **24** (Figure 7) are good building blocks for the monoalkylated

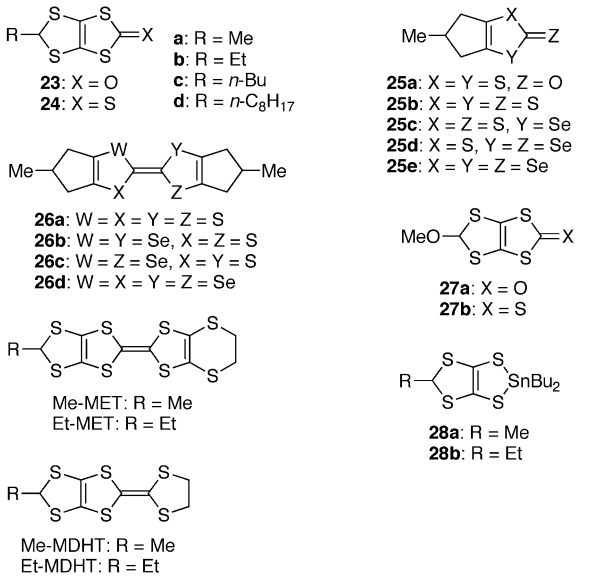

Figure 7.

TTF-type donors. As the related achiral compounds, the methylated 1,3-dichalcogenole-2-chalcogenones **25a**−**e** have been prepared and serve as intermediates or precursors leading to the bis(methyltrimethylene)-substituted TCF derivatives **26a**−**d**.[24] On the other hand, a systematic, practical preparation of **23** or **24** was not realized. We thus investigated the Lewis-acid-promoted alkylation of 1,4-(methoxymethylenedithio)-1,3-dithiole-2-chalcogenones **27a**,**b**, because these compounds contain an orthodithioester moiety that can be expected to be labile under acidic conditions.[25]

Methylation of **27a**,**b** with Me_3Al and ethylation of **27a** with Et_3Al proceeded smoothly to give **23a** (63% yield), **24a** (55% yield), and **23b** (56% yield), respectively. For introduction of the *n*-butyl and *n*-octyl groups into **27a**, use of organometallic/Lewis-acid complex reagents, *n*-BuMgCl/$TiCl_4$ and *n*-$C_8H_{17}MgBr/TiCl_4$, was found to be effective (**23c**, 34% yield; **23d**, 38% yield). The methylated and ethylated TTF donors, Me-MET and Et-MET, were obtained by the $(MeO)_3P$-mediated cross-coupling between **23a**,**b** and thione **8a** (Figure 3) in 66% and 59% yields, respectively. In addition, conversion of **23a**,**b** into tin dithiolates **28a**,**b** followed by the Me_3Al-promoted reaction with 2-ethoxycarbonyl-1,3-dithiolane ($n = 2$ in Scheme 2) gave the methylated and ethylated DHTTF donors, Me-MDHT and Et-MDHT, in 42% and 44% overall yields, respectively.[26]

3. Donor Systems with Extended σ-Bond Framework

Although an additional σ-bond framework appended to a π-donor molecule cannot directly contribute to electrical conduction, it is thought that this addendum certainly leads to a geometrically bulkier structure, which in turn controls intermolecular interaction and enables a novel packing motif. However, it was not clear what kind of σ-bond framework could be used to extend donor molecules with the aim of creating novel donor packing motifs conducive to metallic electronic structures. We have been studying this problem and succeeded in finding some answers. In the following three sections our approach to this problem will be described.

3.1. TTF Donors Extended by Fusion of a Heterocycle

The donor ET (Figure 1), needless to say, produces the largest number of superconducting salts, and it is well known that the additional sulfur atoms, accompanied by fusion of a 1,4-dithiane ring onto both sides of the prototype TTF molecule, play an important part in the formation of 2D S···S contacts in the ET-based superconductors.[2] Accordingly, one promising strategy for the construction of new TTF donors leading to conductive CT materials with enhanced dimensionality might be the fusion of another heterocycle onto the one or two outer rings in the ET-type donors. Moreover, such newly modified TTF donors offer the possibility of forming new packing motifs.

The initial report by Kotov and co-workers on the synthesis of the bis(heterocycle)-fused derivative of ET, BDDT-TTF (Figure 8),[18] has been followed by additional examples of constructing its analogues BDTET,[17] TOET,[27] and compound **29**.[28] Prior to these syntheses, compounds **30** and **31** as the bis(cycloalkane)-fused derivatives of ET had been known.[29] Kini et al. revealed the crystal structure of (*cis*,*cis*-

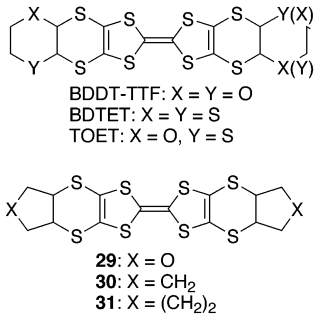

Figure 8.

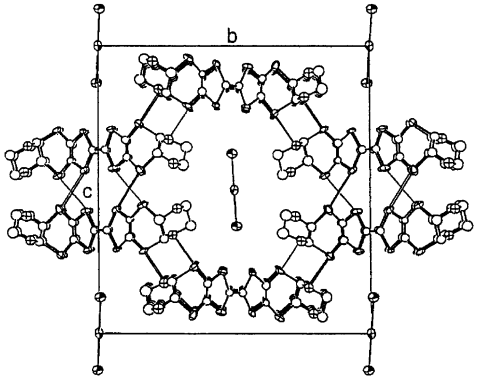

Figure 9. Crystal structure of $(BDDT\text{-}TTF)_2I_3$ viewed along the a-axis. Short S···S and S···O contacts are indicated by thin lines. (Reprinted with permission from ref 30. Copyright 1995, The Royal Society of Chemistry.)

$BDDT\text{-}TTF)_2I_3$ by X-ray analysis.[30] In the salt, a columnar structure instead of the layered structure typical to ET salts occurs and each anion stack is surrounded by four donor molecule double stacks (Figure 9). Unfortunately, the small dimensions and fragile nature of the crystals of this salt hampered the conductivity measurement. Meanwhile, a compressed pellet of the TCNQ complex of TOET showed a conductivity (σ) of 3×10^{-3} S cm^{-1}.[27]

Synthesis of the bis(heterocycle)-fused ET donors via coupling reaction between chalcogenones, e.g., **14a**−**c** (Scheme 6), leads to a mixture of stereoisomers. For example, the formation of two diastereomers of *cis*,*cis*-BDDT-TTF was ascertained by ^{1}H NMR.[18,30] The inherent complication of a stereoisomeric mixture frequently causes difficulties in preparation of single crystals for X-ray studies of both neutral and charged molecules. On the other hand, there exist no stereoisomers in ET derivatives with only one *cis*-fused 1,4-dichalcogenane ring, such as DOET, DOES, and DOEO (Figure 4), owing to the molecular symmetry. We thus began exploring organic metals based on the dioxane-fused derivative of ET, DOET, and its analogues.

The molecular structure of DOET is shown in Figure 10a.[17b] It is obvious that the dioxane ring fused onto the ET molecule makes it bulkier;[31] the same can be said for the seleno analogue of DOET, DOES (Figure 10b), although its molecular structure is not isostructural to that of DOET.[6b] Nevertheless, DOET gave the metallic $Au(CN)_2$ and BF_4 salts,[32] and DOES also formed metallic salts with the I_3^- and AuI_2^- anions.[19a] All these salts underwent metal-to-insulator (MI) transitions at temperatures ranging

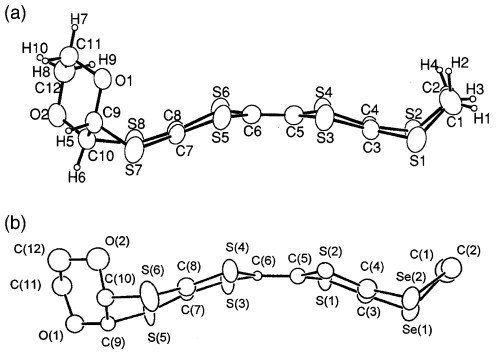

Figure 10. Side views of the molecular structures of DOET (a) and DOES (b) (Reprinted with permission from ref 6b. Copyright 1999, The Royal Society of Chemistry.). In b, the hydrogen atoms are omitted due to their large thermal motions.

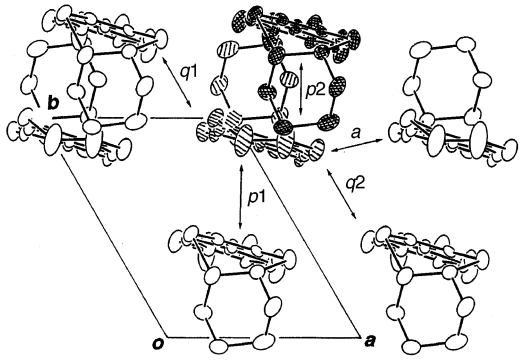

Figure 11. Donor arrangement in $(DOET)_2BF_4$. Intermolecular overlap integrals ($\times 10^{-3}$) a, $p1$, $p2$, $q1$, and $q2$ are −4.66, 23.8, 15.2, 7.05, and 5.34, respectively. (Reprinted with permission from ref 32. Copyright 1997, The Royal Society of Chemistry.)

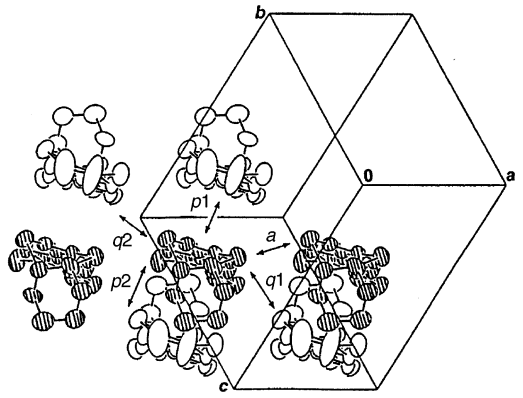

Figure 12. Donor arrangement in $(DOES)_2(AuI_2)_{0.75}$. Intermolecular overlap integrals ($\times 10^{-3}$) a, $p1$, $p2$, $q1$, and $q2$ are −3.15, 21.3, 22.7, 7.51, and 8.51, respectively. (Reprinted with permission from ref 19a. Copyright 1998, The Royal Society of Chemistry.)

from 250 to 30 K. The metallic $(DOET)_2BF_4$ and $(DOES)_2(AuI_2)_{0.75}$ salts showed room-temperature σ's (σ_{rt}'s) of 27 and 1.4 S cm^{-1}, respectively, and their X-ray analyses established that these salts have β-type donor arrangements (Figures 11 and 12) similar to that found in a superconductor β-$(ET)_2I_3$.[33] In the β-structure, dimerization of donor molecules occurs usually within a stack. Considering that the overlap integral ratios of $p1$ to $p2$ in β-$(ET)_2I_3$, $(DOET)_2BF_4$, and $(DOES)_2(AuI_2)_{0.75}$ are 2.9,[33c] 1.6, and

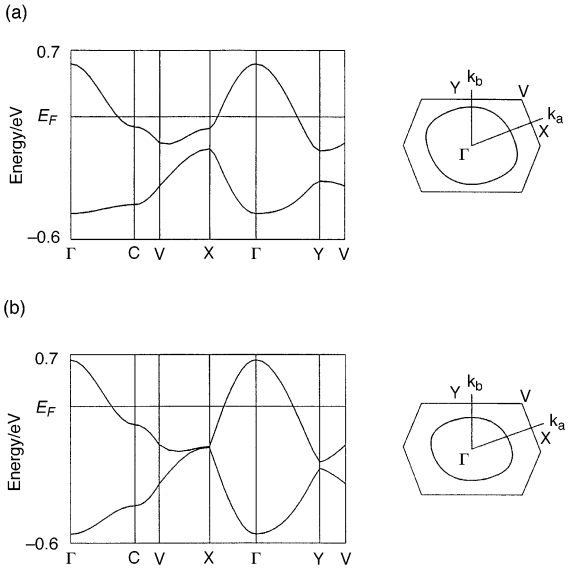

Figure 13. Energy band structures and Fermi surfaces of $(DOET)_2BF_4$ (a) (Reprinted with permission from ref 6b. Copyright 1999, The Royal Society of Chemistry.) and $(DOES)_2(AuI_2)_{0.75}$ (b) (Reprinted with permission from ref 19a. Copyright 1998, The Royal Society of Chemistry.).

0.94, respectively,[34] dimerization in $(DOET)_2BF_4$ is smaller than that in β-$(ET)_2I_3$ and the donor stack in $(DOES)_2(AuI_2)_{0.75}$ is more uniform than that in $(DOET)_2BF_4$. Intermolecular A···A (A = atom) contacts shorter than the sum of the van der Waals radii are known to be important in studying electronic structures of organic conductors. In $(DOET)_2BF_4$, instead of no short S···S contact (< 3.70 Å) in a stack, there are many short S···S contacts between stacks. A similar chalcogen···chalcogen contact pattern is observed in $(DOES)_2(AuI_2)_{0.75}$. These contact patterns reflect 2D band structures with nearly isotropic closed Fermi surfaces (Figure 13a,b). However, the $(DOET)_2BF_4$ salt turned semiconductive around 100 K. According to the X-ray analysis, the orientation of BF_4^- anions is completely disordered, so this random potential of BF_4^- anion layers could disturb the electron conduction and make this salt semiconductive at low temperatures. The conduction band of $(DOET)_2BF_4$ is 3/4 filled, whereas the band filling of $(DOES)_2(AuI_2)_{0.75}$ increases by 8.3% compared to that of $(DOET)_2BF_4$. Consequently, the area of the Fermi surface of $(DOES)_2(AuI_2)_{0.75}$ is smaller than that of $(DOET)_2BF_4$.

Kotov and co-workers subsequently reported a series of metallic DOET salts with HSO_4^-, FSO_3^-, $Hg_2Br_6^{2-}$, $Hg_2Cl_6^{2-}$, NO_3^-, and SiF_5^- anions.[35] It is noteworthy that the Hg_2Cl_6 salt ($\sigma_{rt} = 10-60$ S cm^{-1}) retained the metallic state down to 4 K. The crystal structure of $(DOET)_4Hg_2Cl_6$ was determined by X-ray analysis. In the salt, short O···Cl and H···Cl contacts are observed between anions and donor molecules in addition to many short S···S contacts between donor stacks (Figure 14). Meanwhile, we found that the oxo analogue of DOET, DOEO (Figure 4), produces the metallic $Au(CN)_2$, BF_4, and PF_6 salts stable down to 2 K.[19b,c] By X-ray analysis, donor molecules in $(DOEO)_2BF_4$ (σ_{rt} = 27 S cm^{-1}) were ascertained to form the β''-type packing motif (Figure 15) in which there are short S···O contacts as well as short S···S

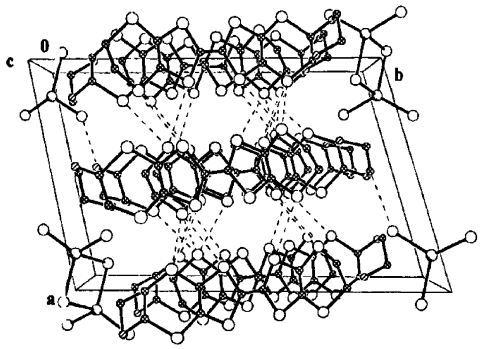

Figure 14. Crystal structure of $(DOET)_4Hg_2Cl_6$. Broken lines indicate short S···S, O···Cl, and H···Cl contacts. (Reprinted with permission from ref 35. Copyright 2001, Elsevier.)

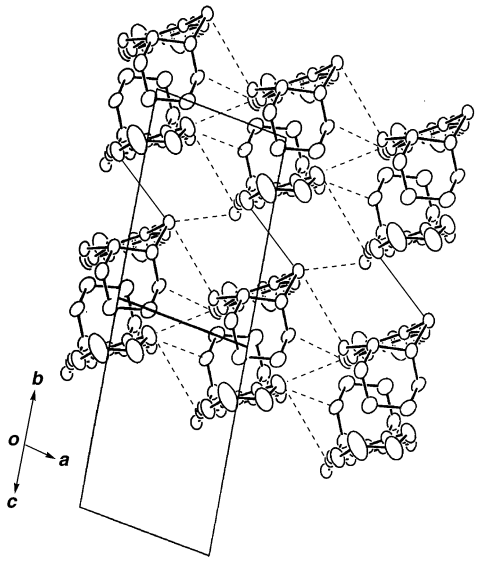

Figure 15. Donor arrangement in $(DOEO)_2BF_4$. Short interstack S···S and S···O contacts are shown by broken lines, whereas thin lines indicate short intrastack S···S contacts.

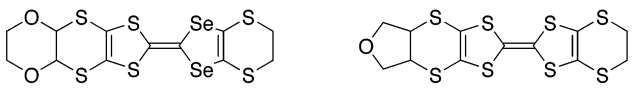

32 33

Figure 16.

contacts between stacks. Notably, short S···S contacts occur within a stack, which is in contrast to the fact that no short intrastack S···S contacts are observed in $(DOET)_2BF_4$ and $(DOES)_2(AuI_2)_{0.75}$. Although the selenium-containing and THF-fused analogues of DOET, i.e., compounds **32**[19c] and **33**[28] (Figure 16), have so far failed to provide any metallic CT materials, a semiconducting 1:1 (donor:anion) salt, **33**·$Au(CN)_2$ ($\sigma_{rt} = 3 \times 10^{-3}$ S cm^{-1}), was reported to have a sandwiched structure in which an anion is located between two donor molecules.

3.2. TTF Donors Linking a Heterocycle

It is surprising that a compressed pellet of the TCNQ complex of DO-MET (Scheme 7) exhibited metallic conducting behavior with σ_{rt} = 12 S cm^{-1} [20] because the molecular structure of DO-MET is considerably bulkier than that of its structural isomer

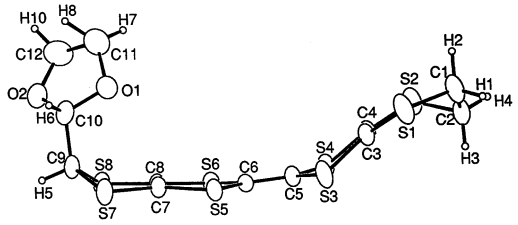

Figure 17. Side view of the molecular structure of DO-MET. (Reprinted with permission from ref 20. Copyright 1997, Elsevier.)

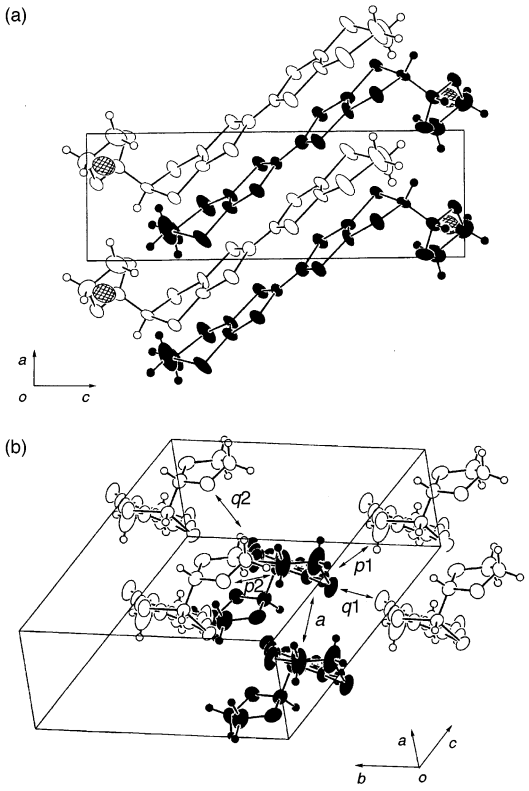

Figure 18. (a) Crystal structure of $(DO\text{-}MET)_2AsF_6$. The front molecules shown by darkly shaded circles are stacked head-to-head with a constant interplanar spacing of 3.70 Å. The As atoms are indicated by reticulated circles. (b) Donor arrangement in $(DO\text{-}MET)_2AsF_6$. Intermolecular overlap integrals ($\times 10^{-3}$) a, $p1$, $p2$, $q1$, and $q2$ are 3.27, 14.2, 9.34, −13.3, and 12.2, respectively.

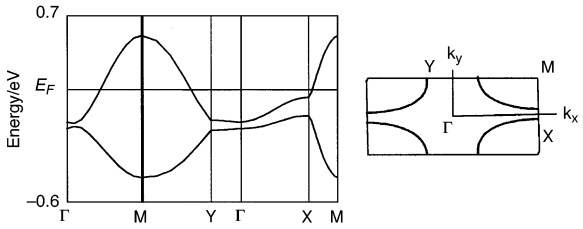

Figure 19. Energy band structure and Fermi surface of $(DO\text{-}MET)_2AsF_6$.

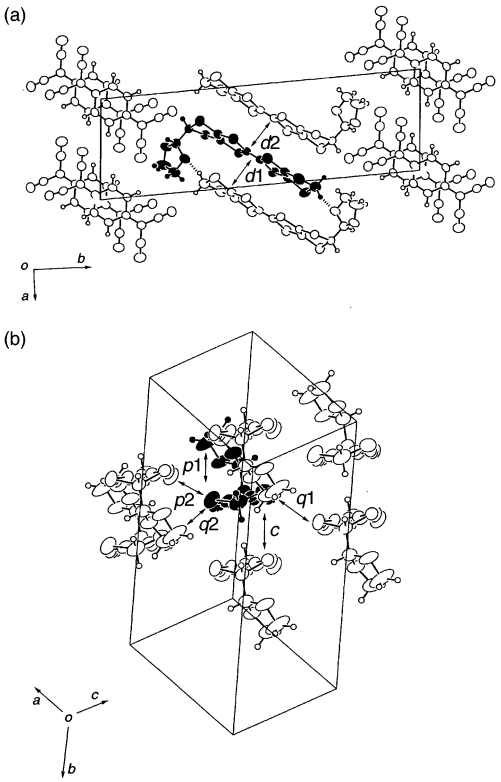

Figure 20. (a) Crystal structure of (DO-MMT)(TCNQ). Intermolecular hydrogen bonds [3.251(6) Å] are indicated by dashed lines. Interplanar distances in the DO-MMT column are 3.67 ($d1$) and 3.65 ($d2$) Å, and those in the TCNQ column are 3.34 and 3.26 Å. (b) Donor arrangement in (DO-MMT)(TCNQ). Intermolecular overlap integrals ($\times 10^{-3}$) c, $p1$, $p2$, $q1$, and $q2$ are 10.4, 20.3, 12.6, 20.4, and −1.95, respectively.

DOET (Figure 10a) due to the presence of the dioxolane ring almost perpendicularly bonded to the curved MET[36] moiety (Figure 17). Further exploration of the conductive DO-MET salts revealed that the BF_4 ($\sigma_{rt} = 22$ S cm^{-1}) and AsF_6 ($\sigma_{rt} = 9.4$ S cm^{-1}) salts are metallic down to 2.6 and 2.0 K, respectively.[21b] The crystal structure of $(DO\text{-}MET)_2AsF_6$ is depicted in Figure 18. In the salt, the DO-MET molecules are stacked along the a-axis in a head-to-head manner with a constant interplanar spacing of 3.70 Å and also to a considerable extent mutually shifted so as to avoid the steric hindrance of the dioxolane ring (Figure 18a). Nevertheless, the value of the intrastack overlap integral (corresponding to a) is appreciable though smaller than those of the interstack overlap integrals $p1$, $p2$, $q1$, and $q2$ (Figure 18b), thereby leading to the 2D energy dispersion relation and Fermi surface (Figure 19) similar to those calculated for a τ-type conductor in which the conduction band is supposed to be 3/4 filled.[37] Another point worth noting is that such a head-to-head stacking mode formed by unsymmetrical donor molecules can rarely be found.[38]

Oxygen-containing substituents are expected to enable intermolecular hydrogen bonding. In contrast to the head-to-head donor stack observed in $(DO\text{-}MET)_2AsF_6$, a head-to-tail donor stack to which intermolecular hydrogen bonds make an important contribution occurred in the TCNQ complex of DO-MMT (Figure 6) with a 1:1 stoichiometry.[21b] From the results of the variable-temperature conductivity and thermoelectric power measurements, it was elucidated that (DO-MMT)(TCNQ), with $\sigma_{rt} = 63$ S cm^{-1}, exhibits hole conduction in the metallic-like state around room temperature and a transition to the semiconductive state below ca. 280 K. As illustrated in Figure 20a, the crystal structure of the complex consists of alternating layers containing only DO-

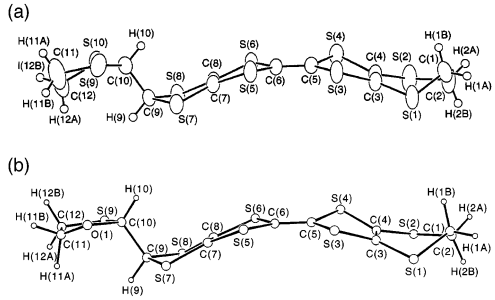

Figure 21. Side views of the molecular structures of DT-MET (a) (Reprinted with permission from ref 21a. Copyright 1998, Elsevier.) and OT-MET (b). The OT-MET molecules crystallized as a 1:1 racemic mixture.

MMT molecule and only TCNQ molecule. The donor layer contains the DO-MMT dimers in which two DO-MMT molecules are connected through two C−H···O hydrogen bonds and adopts the β-packing arrangement. Formation of the hydrogen-bonded dimer is understood by considering that the DO-MMT molecule has the relatively acidic methylene group activated by two sulfur atoms. There are some large overlap integrals between donor stacks as well as within a donor stack (Figure 20b), suggestive of a 2D conducting layer responsible for the metallic-like behavior. On the other hand, TCNQ molecules form one-dimensional (1D) stacks along the *c*-axis with some dimerization, which appears to cause the transition to semiconducting behavior.

Replacement of one or two oxygen atoms of the dioxolane ring in DO-MET with sulfur might promote increased dimensionality. From this point of view, we undertook the study of the dithiolane and oxathiolane analogues of DO-MET, DT-MET and OT-MET (Figure 6).[21]

Figure 21a,b shows the molecular structures, which are isostructural with each other. Both structures are nonplanar but less bulky than that of DO-MET (Figure 17). Analogous to DO-MET, DT-MET produced several metallic salts, i.e., the metallic AuI_2 (σ_{rt} = 13 S cm^{-1}), BF_4 (σ_{rt} = 7.0 S cm^{-1}), PF_6 (σ_{rt} = 1.5 S cm^{-1}), and AsF_6 (σ_{rt} = 19 S cm^{-1}) salts with MI transition temperatures of 35−110 K. However, the quality of single crystals of these salts fell short of successful X-ray analyses. The racemic OT-MET donor also gave the metallic BF_4 salt (σ_{rt} = 7.5 S cm^{-1}) despite the fact that the variable-temperature resistivity was measured on a compressed pellet.

In this way, production of metallic CT materials from the dichalcogenolane-linked TTF donors became feasible. Our attention was thus focused on elucidating whether TTF donors with a larger heterocycle than the dichalcogenolane ring provide metallic CT materials. To this end, we chose to undertake the preparation of CT materials based on the dichalcogenane derivatives of MET, DOA-MET and DTA-MET (Figure 6).[22]

By X-ray analysis it was revealed that the dioxane ring in the neutral DOA-MET molecule is bonded to the MET moiety in an equatorial-like manner and favors a chair conformation (Figure 22). The entire molecular structure of DOA-MET is evidently planar compared to that of DO-MET with the dioxolane ring located at the axial-like position (Figure 17). In the

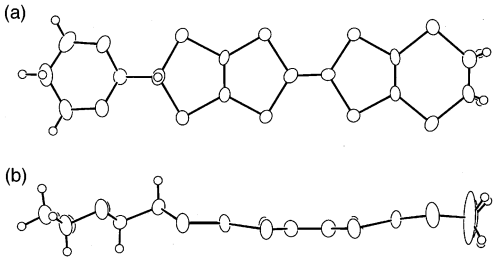

Figure 22. Top (a) and side (b) views of the molecular structure of DOA-MET. (Reprinted with permission from ref 22. Copyright 2001, The Chemical Society of Japan.)

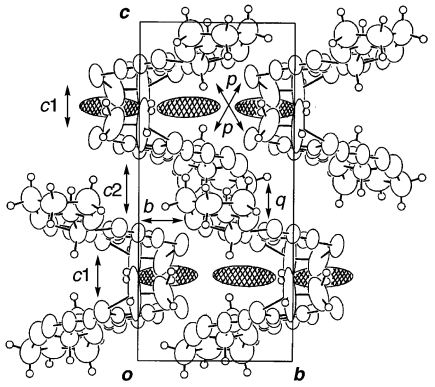

Figure 23. Crystal structure of $(DOA\text{-}MET)_3AuI_2$. Intermolecular overlap integrals ($\times 10^{-3}$) *c*1, *c*2, *b*, *q*, and *p* are 6.73, −3.24, 10.9, 16.7, and 2.04, respectively. Reticulated circles indicate the AuI_2 anions, which lie parallel to the *b*-axis with the periodicity of 3/2*b*. (Reprinted with permission from ref 22. Copyright 2001, The Chemical Society of Japan.)

series of the DOA-MET salts so far prepared, only the resistivity of the AuI_2 salt (σ_{rt} = 6.5 S cm^{-1}) upon cooling from room temperature to ca. 180 K exhibited weak metallic behavior and then a gradual change to semiconducting behavior upon further cooling. On the other hand, all the DTA-MET salts with linear (I_3^- and AuI_2^-), tetrahedral (BF_4^- and ClO_4^-), and octahedral (PF_6^- and AsF_6^-) anions were semiconductors (σ_{rt} = 10^0 to 10^{-3} S cm^{-1}) with activation energies (E_a's) ranging from 34 to 72 meV.

X-ray analysis of the AuI_2 salt of DOA-MET revealed that the salt has a 3:1 donor-to-anion ratio and a β-type donor arrangement similar to that observed in β-$(ET)_2PF_6$.[39] Figure 23 shows its crystal structure in which the DOA-MET molecules form two consecutive pairs (Figure 24) to stack along the *c*-axis in a screwed fashion. Although the planar structure of DOA-MET that can be found in the neutral state remains almost unchanged, there is no short S···S contact within a screwed stack. The value of the intrastack overlap integral *c*2 is also small, which reflects an unfavorable molecular overlap as shown in Figure 24b. On the other hand, three short S···S contacts are observed between stacks along the direction shown by the interstack overlap integral *b* in Figure 23. These anisotropic interactions in the donor layer lead to a 1D electronic structure in which the Fermi surface is open along the screwed intrastacking *c* direction but closed along the interstacking *b* direction (Figure 25). Judging from the electronic structure, this salt is expected to undergo the Peierls transition peculiar to the 1D character. However,

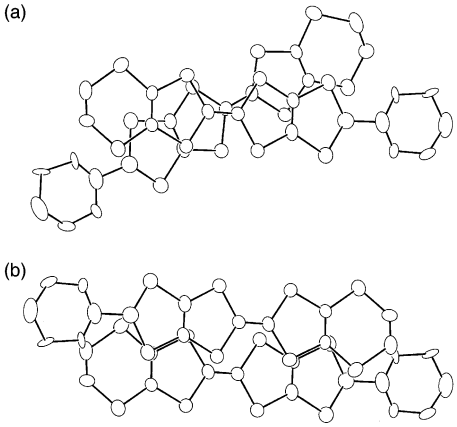

Figure 24. Projection views of two donor pairs in a stack along the $c1$ (a) and $c2$ (b) directions shown in Figure 23. (Reprinted with permission from ref 22. Copyright 2001, The Chemical Society of Japan.)

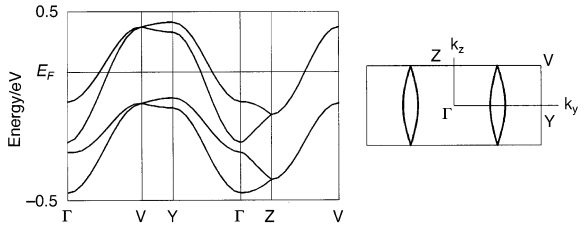

Figure 25. Energy band structure and Fermi surface of $(DOA\text{-}MET)_3AuI_2$. (Reprinted with permission from ref 22. Copyright 2001, The Chemical Society of Japan.)

unlike a sharp MI transition of β-$(ET)_2PF_6$ associated with the Peierls-type (charge density wave) distortion,[39b] a broad transition was observed in the variable-temperature resistivity measurement of this salt. Therefore, the origin of the gradual change to semiconducting behavior is currently unknown.

3.3. Monoalkylated TTF Donors

As described above, linkage of a heterocycle, especially a dichalcogenolane ring, to the MET molecule proved to be an unprecedented structural modification to obtain organic metals since the parent MET donor has been reported to yield the semiconducting ClO_4, PF_6, and ReO_4 salts.[40] This result prompted exploration of the metallic CT materials based on the monoalkylated derivatives of MET, Me-MET and Et-MET (Figure 7).[25]

While the temperature dependence of the resistances for single crystals of the Me-MET salts with AuI_2^-, BF_4^-, ClO_4^-, and PF_6^- anions was semiconductive ($\sigma_{rt} = 10^{-1}$ to 10^{-4} S cm^{-1}, $E_a = 120-230$ meV), compressed pellets of the ClO_4 ($\sigma_{rt} = 26$ S cm^{-1}) and PF_6 ($\sigma_{rt} = 17$ S cm^{-1}) salts of Et-MET exhibited metallic behavior. This is noteworthy because the Et-MET donor, relative to Me-MET, has a longer alkyl chain. Further investigation of the synthesis of other monoalkylated TTF donors and structural characterization of derived CT materials is actively in progress.

4. Donor Systems with Reduced π-Electron System

In the molecular design of π-donors for developing new organic metals and superconductors, it is predicted that partial reduction of the π-system of a donor molecule would adversely affect the electron-donating ability and the on-site Coulombic repulsion and, consequently, would be deemed crucial in forming the segregated stacking of donor molecules in CT complexes or salts. However, this prediction does not always apply to any case as illustrated below.

4.1. DHTTFs

In 1971 Coffen and co-workers reported the synthesis and electrochemical properties of the parent DHTTF molecule (Figure 1).[41] Formation of DHTTF, albeit as a minor product, was achieved by DDQ oxidation of 2,2′-bi(1,3-dithiolanyl) in boiling toluene (Scheme 10). The major product in the reaction was 2,2′-bis(1,3-dithiolanylidene). An alternative synthetic method for the exclusive formation of DHTTF reported by Mori et al. involved reaction of bis(dimethylaluminum) *cis*-1,2-ethylenedithiolate with 2-ethoxycarbonyl-1,3-dithiolane (Scheme 10).[42]

Scheme 10

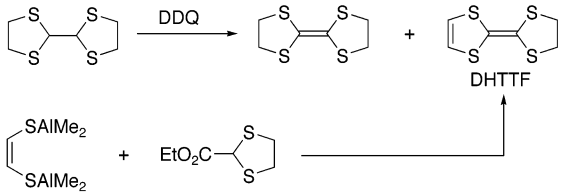

DHTTF, like TTF, has been found to show two pairs of reversible redox waves by cyclic voltammetry (CV).[41] On comparing the respective values of oxidation potentials for DHTTF [$E_1 = +0.405$, $E_2 = +0.89$, ΔE $(E_2 - E_1) = 0.485$ V (vs SCE)] with those for TTF [$E_1 = +0.33$, $E_2 = +0.70$, ΔE $(E_2 - E_1) = 0.37$ V], the first oxidation potential (E_1, representing the electron-donating ability) of DHTTF is shifted to a more positive value compared with that of TTF and the difference between the first and second oxidation potentials [ΔE $(E_2 - E_1)$, corresponding to the magnitude of the on-site Coulombic repulsion] in DHTTF is larger than that in TTF, suggesting that both oxidation of DHTTF and generation of its dicationic state are more difficult. Presumably these drawbacks as a π-electron donor would hinder the challenging task of synthesizing a variety of DHTTFs, except for several derivatives that have been summarized as part of our earlier review,[6d] in striking contrast to a large number of chemical modifications to TTF. However, this situation might change with our findings of (i) the metallic AuI_2 salt of MDHT (Figure 2)[10b,26] and (ii) the superconducting AsF_6, PF_6, and $BF_4{\cdot}H_2O$ salts of DODHT (vide infra, Scheme 11).[43]

4.1.1. MDHT and Its Conductive Salts

As expected, the donor MDHT showed a higher E_1 value [+0.60 V (vs SCE) in CH_3CN] and a larger ΔE $(E_2 - E_1)$ value (0.40 V) compared to the corresponding values of its TTF analogue MDT-TTF [Figure 2, $E_1 = +0.49$, ΔE $(E_2 - E_1) = 0.29$ V].[10b] Nevertheless, MDHT with AuX_2^- (X = CN, Cl, Br, and I) anions formed CT salts which exhibited high σ_{rt}'s on the order of 10^0 to 10^2 S cm^{-1} for single crystals or

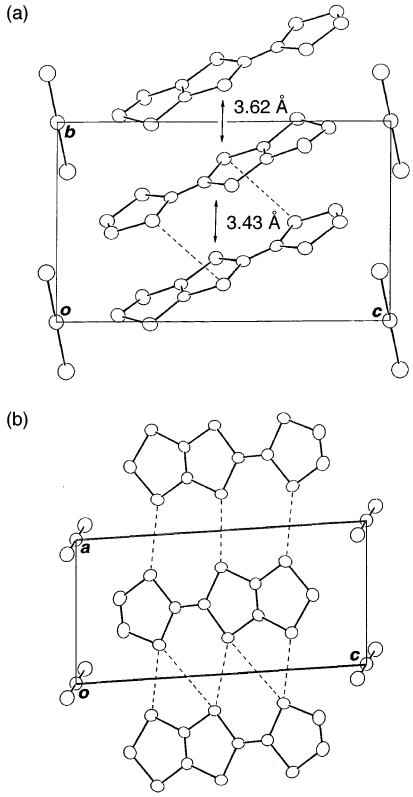

Figure 26. Crystal structure of $(MDHT)_2AuCl_2$ viewed along the *a*-axis (a) and the *b*-axis (b). Short S···S contacts are indicated by broken lines. (Reprinted with permission from ref 6b. Copyright 1999, The Royal Society of Chemistry.)

compressed pellets.[6b,44] In particular, the $(MDHT)_2AuI_2$ salt (σ_{rt} = 60 S cm^{-1}) remained metallic all the way down to 1.4 K, although the π-system of MDHT is less extended than that of MDT-TTF. The other AuX_2 (X = CN, Cl, and Br) salts were semiconductors with small E_a's of 6−20 meV.

The crystal structure of a small gap semiconductor $(MDHT)_2AuCl_2$ (σ_{rt} = 250 S cm^{-1}, E_a = 6 meV) was determined by X-ray analysis.[6b,44] As shown in Figure 26a, the salt consists of alternate layers of MDHT donor molecules arranged in the β-packing mode and layers of $AuCl_2^-$ anions. In the donor layer, there exist several short S···S contacts between donor stacks (Figure 26b). On the other hand, within a donor stack, dimerization of donor molecules is somewhat large (interplanar distances of 3.62 and 3.43 Å) and deviation of the overlap of two donor molecules with an interplanar spacing of 3.62 Å is also comparatively large. The dimerization and deviation may be responsible for the semiconductive behavior of this salt.

According to structural information on the metallic $(MDHT)_2AuI_2$ salt, the salt also contains layers of donor molecules alternating with anion layers (Figure 27a).[26] The donor molecule packing is similar to that found in a superconductor θ-$(ET)_2I_3$ (Figure 27b).[45] For θ-type ET conductors, Mori and coworkers proposed a phase diagram as a function of the dihedral angle between the planes formed by donor molecules on adjacent stacks.[46] The corresponding dihedral angle of $(MDHT)_2AuI_2$ is 101.8°, which belongs to the same category with θ-$(ET)_2I_3$

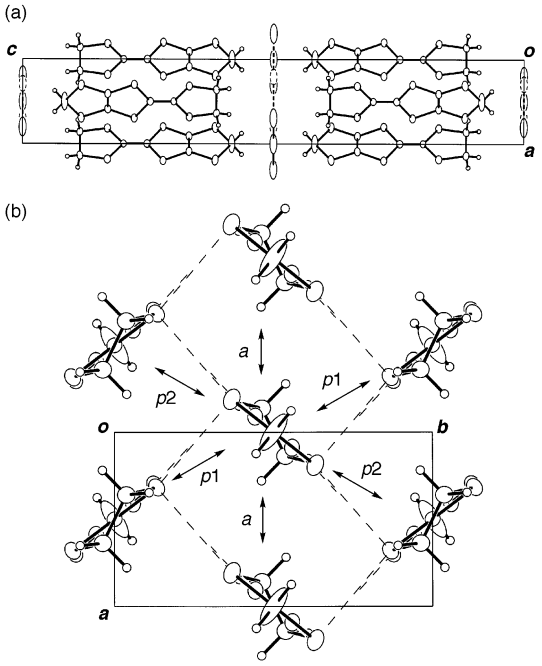

Figure 27. (a) Crystal structure of $(MDHT)_2AuI_2$ viewed along the *b*-axis. For the Au site, two independent positions depicted by open and broken circles, respectively, are observed. The respective occupancies are distributed to 0.670(3) for open circles and 0.1651(25) for broken circles. (b) Donor arrangement in $(MDHT)_2AuI_2$. Short S···S contacts are drawn by broken lines. Intermolecular overlap integrals ($\times 10^{-3}$) *a*, *p*1, and *p*2 are −1.46, −14.5, and −14.3, respectively.

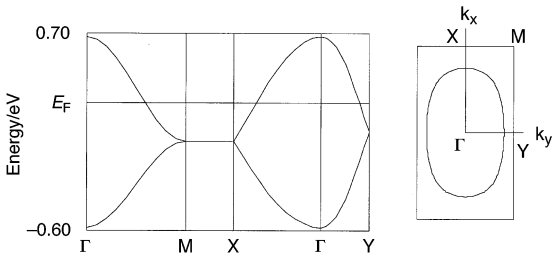

Figure 28. Energy band structure and Fermi surface of $(MDHT)_2AuI_2$.

(99°) and θ-$(ET)_2Ag(CN)_2$ (101°). Several short S···S contacts are observed between stacks, whereas there is no short S···S contact within a stack; a similar S···S contact pattern can be found in θ-$(ET)_2I_3$.[45b] The large overlap integrals are also calculated between stacks, suggesting 2D interaction in the donor layer. In fact, the tight-binding band calculation results in the 2D band structure (Figure 28); however, the Fermi surface is less round than that of θ-$(ET)_2I_3$.[45b] The calculated band structure provides support for the metallic conductivity down to a very low temperature.

4.1.2. DODHT Superconductors

As described above, the $(MDHT)_2AuI_2$ salt was found to be metallic down to 1.4 K but failed to develop superconductivity. Therefore, further structural modification to the DHTTF donors we synthesized was required to achieve superconductivity. We thus designed a derivative of EDHT (Figure 2) with the appended dioxane ring by cis fusion, viz., DODHT

(vide infra, Scheme 11), because the *cis*-fused dioxane ring, though bulky, on TTF derivatives does not prevent the formation of metallic electronic structures, as can be found in $(DOET)_2BF_4$,[32] $(DOET)_4Hg_2Cl_6$,[35] $(DOES)_2(AuI_2)_{0.75}$,[19a] and $(DOEO)_2BF_4$.[19b,c] Such a bulky donor containing only a DT unit as a π-system does not appear to hew to the conventional line of the molecular design of π-donors capable of providing superconductors; hence, successful production of DODHT-based superconductors will lead to a new approach in the design of organic superconductors.

Scheme 11

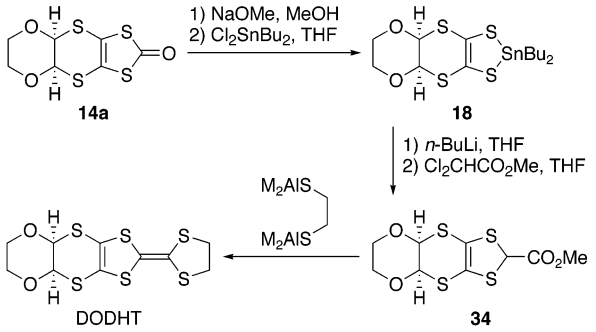

Our synthetic sequence for constructing DODHT is outlined in Scheme 11.[43a,b] Conversion of oxone **14a** into tin dithiolate **18** followed by sequential treatment with *n*-BuLi (2 equiv) and methyl dichloroacetate in THF gave ester **34** in 74% overall yield from **14a**. Reaction of **34** with bis(dimethylaluminum) 1,2-ethanedithiolate led to DODHT in 46% yield, X-ray analysis of which confirmed the cis stereochemistry of the junction on the dioxane ring (Figure 29).[43b] The CV of DODHT showed two pairs of

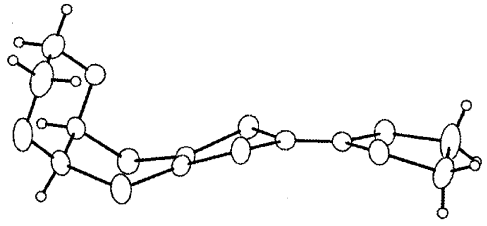

Figure 29. Side view of the molecular structure of DODHT. (Reprinted with permission from ref 43b. Copyright 2003, Elsevier.)

reversible redox waves at +0.64 (E_1) and +1.08 (E_2) V (vs SCE). The E_1 value is higher than that of its TTF analogue DOT (Figure 4, +0.51 V), and the ΔE ($E_2 - E_1$) value (0.44 V) is larger than that of DOT (0.33 V). Figure 30 shows the highest occupied molecular orbital (HOMO) of the DODHT molecule by ab initio calculation (RHF/6-31G**) together with that of the DOT molecule.[6d] In the HOMO of DODHT,

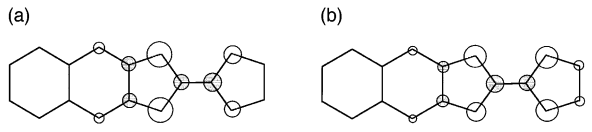

Figure 30. HOMOs of DODHT (a) and DOT (b). (Reprinted with permission from ref 6d. Copyright 2004, Kodansha & Springer.)

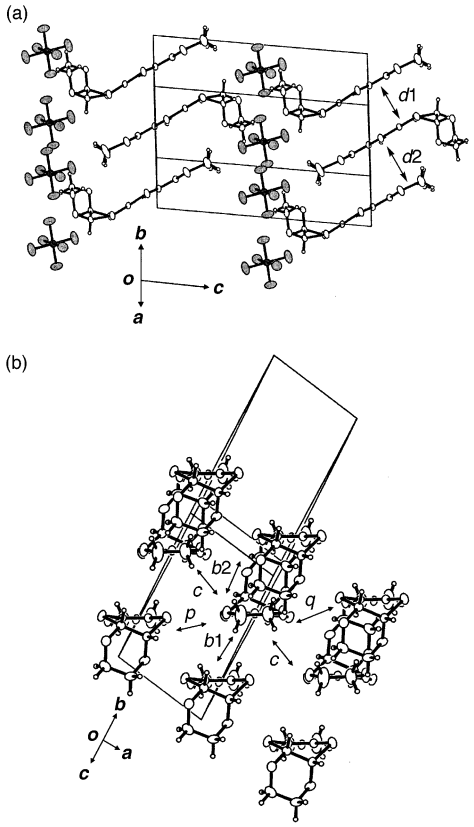

Figure 31. (a) Crystal structure of $(DODHT)_2AsF_6$. Interplanar distances in the DODHT column are 3.73 ($d1$) and 4.00 ($d2$) Å. (b) Donor arrangement in $(DODHT)_2AsF_6$. Intermolecular overlap integrals ($\times 10^{-3}$) $b1$, $b2$, c, p, and q are −2.81, −0.09, −10.95, −10.08, and −6.28, respectively. (Reprinted with permission from ref 6d. Copyright 2004, Kodansha & Springer.)

the atomic orbital coefficients of two sulfur atoms on the 1,3-dithiole ring are larger than those on the 1,3-dithiolane ring, whereas almost the same coefficients are observed for four sulfur atoms on the TTF backbone in the HOMO of DOT.

X-ray analyses of the AsF_6 and PF_6 salts of DODHT established that both salts crystallize isostructurally and have the β''-type (or β''_{211}-type[47]) donor arrangement.[43a,b] Figure 31a shows the crystal structure of $(DODHT)_2AsF_6$ [6d] in which the donor molecules are stacked head-to-tail along the *b*-axis. The interplanar distances (3.73 and 4.00 Å) within the stack are much longer than those in the metallic $(DOET)_2BF_4$ (3.50 and 3.77 Å) and $(DOES)_2(AuI_2)_{0.75}$ (3.47 and 3.78 Å) salts. There are several short S···S contacts between stacks, whereas no short S···S contact is observed within a stack. This S···S contact pattern reflects the anisotropy of the overlap integrals (Figure 31b), suggesting that the transverse interaction is superior to the interaction within the stack. Moreover, the two donor molecules with an interplanar spacing of 4.00 Å are mutually slipped along both molecular short and long axes, which causes the overlap integral $b2$ to be almost zero. These structural characteristics also hold for the isostructural $(DODHT)_2PF_6$.

The resistivities of $(DODHT)_2AsF_6$ ($\sigma_{300K} = 1.2$ S cm^{-1}) as a function of temperature under various pressures are shown in Figure 32a. At ambient pressure, the resistivity was semiconductive with a

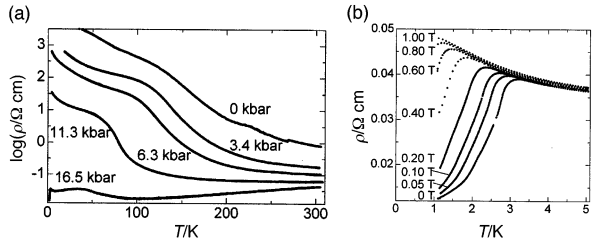

Figure 32. (a) Temperature dependence of the resistivities for $(DODHT)_2AsF_6$ at pressures of 0−16.5 kbar. (b) Magnetic field dependence of the superconducting transition of $(DODHT)_2AsF_6$ at 16.5 kbar.

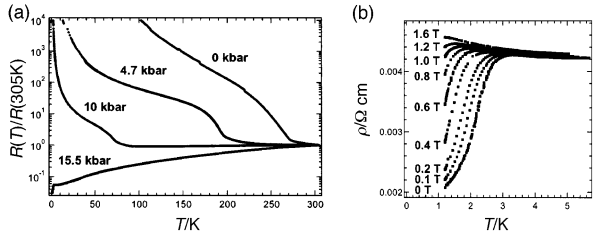

Figure 33. (a) Temperature dependence of the resistivities for $(DODHT)_2BF_4{\cdot}H_2O$ at pressures of 0−15.5 kbar. (b) Magnetic field dependence of the superconducting transition of $(DODHT)_2BF_4{\cdot}H_2O$ at 15.5 kbar. (Reprinted with permission from ref 43c. Copyright 2003, The Royal Society of Chemistry.)

broad shoulder around 120 K, and with increasing pressure, pronounced humps appeared at lower temperatures. At 16.5 kbar, the resistivity exhibited metallic behavior below room temperature and an abrupt drop attributed to a superconducting transition with an onset of 3.3 K. Superconductivity in this salt was confirmed by the magnetic field dependence of the drop of the resistivity measured at 16.5 kbar. With increasing magnetic field, the superconducting transition of this salt shifted to a lower temperature and was suppressed under 1 T (Figure 32b). Similar to the $(DODHT)_2AsF_6$ salt, $(DODHT)_2PF_6$ ($\sigma_{300K} = 9.2 \times 10^{-1}$ S cm^{-1}) exhibited semiconducting behavior at ambient pressure and metallic behavior at 11.3 kbar, then underwent a superconducting transition with an onset of 3.1 K at 16.5 kbar, which disappeared under an applied magnetic field of 1 T.

Besides the isomorphous superconductors $(DODHT)_2X$ (X = AsF_6 and PF_6) under applied pressures, the $(DODHT)_2BF_4{\cdot}H_2O$ hydrate ($\sigma_{rt} = 2.8$ S cm^{-1}) was found to undergo a superconducting transition at 3.2 K under a hydrostatic pressure of 15.5 kbar (Figure 33a).[43c] The temperature dependence of the resistivities under magnetic fields of up to 1.6 T at 15.5 kbar indicated that the superconducting transition disappears completely under 1.6 T (Figure 33b). This result provides evidence of superconductivity in $(DODHT)_2BF_4{\cdot}H_2O$. Thus, it is concluded that the hydrate is one of the few superconducting salts to contain water.[48] Figure 34a shows its crystal structure which consists of alternating layers of DODHT molecules and layers containing BF_4^- and H_2O. Although the donor molecule packing belongs to the β''-type category similar to those of $(DODHT)_2X$ (X = AsF_6 and PF_6), the crystal structure is by no means isostructural to those of the AsF_6 and PF_6 salts. There are two crystallographically independent donor molecules which are stacked with a

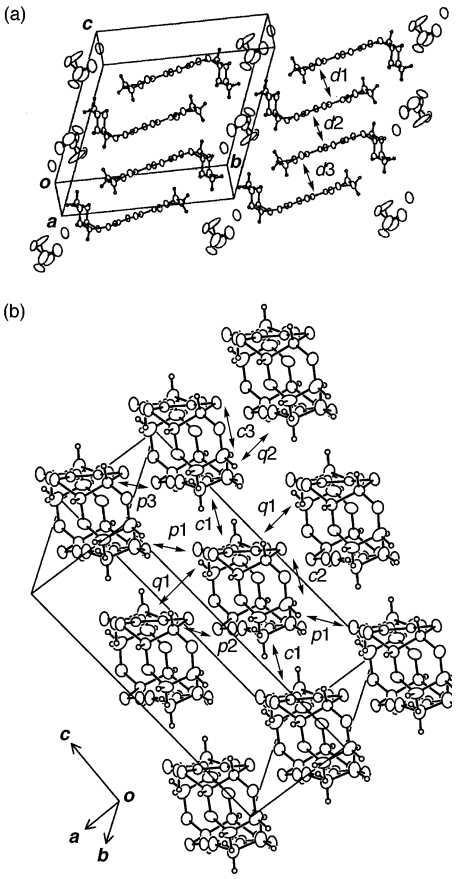

Figure 34. (a) Crystal structure of $(DODHT)_2BF_4{\cdot}H_2O$. Interplanar distances in the DODHT column are 3.85 ($d1$), 3.57 ($d2$), and 3.81 ($d3$) Å. (b) Donor arrangement in $(DODHT)_2BF_4{\cdot}H_2O$. Intermolecular overlap integrals ($\times 10^{-3}$) $c1$, $c2$, $c3$, $p1$, $p2$, $p3$, $q1$, and $q2$ are 0.77, −1.99, −1.89, 11.04, −9.81, −8.54, −10.84, and −12.35, respectively. (Reprinted with permission from ref 43c. Copyright 2003, The Royal Society of Chemistry.)

4-fold period to form two types of cyclic-like pairs with interplanar distances of 3.85, 3.57, and 3.81 Å. The overlap integrals calculated on the donor layer suggest that the interaction within a stack is much weaker than that between stacks (Figure 34b); the similarity can be found in the AsF_6 and PF_6 salts. However, unlike these salts, the respective absolute values of the overlap integrals within the two cyclic-like donor pairs ($c2 = 1.99 \times 10^{-3}$ and $c3 = 1.89 \times 10^{-3}$) are larger than that between these pairs ($c1 = 0.77 \times 10^{-3}$). This is probably due to an only slight difference in the deviation of overlap of donor molecules, which cause an appreciable change in the effective area of the π-system of DODHT that is capable of overlapping. Thus, in the DODHT superconductors, such a subtle variation in the donor arrangements has a marked influence on the intermolecular interaction.

The common noticeable feature of the $(DODHT)_2X$ (X = AsF_6, PF_6, and $BF_4{\cdot}H_2O$) superconductors is that they all exhibit various aspects of the pressure-induced conducting behavior, including semiconducting, metallic, and superconducting phases. It is therefore an important subject of continued interest to clarify how structural change is brought about by applied pressures.

4.1.3. Monoalkylated MDHT Donors

As described in section 3.3, there is a possibility of obtaining organic metals by introducing an alkyl group into a TTF donor. Accordingly, the intriguing question of whether the use of an alkyl group as a σ-bond framework to extend DHTTF donors is recognized as a favorable strategy for developing new organic metals arose quite naturally. We thus attempted to find an answer to the question by pursuing investigation of the methylated and ethylated MDHT donors Me-MDHT and Et-MDHT (Figure 7).[26]

Recrystallization of Me-MDHT gave needlelike and prismatic single crystals, X-ray analyses of which were undertook to compare with the molecular structure of MDHT (Figure 35a). In a needlelike

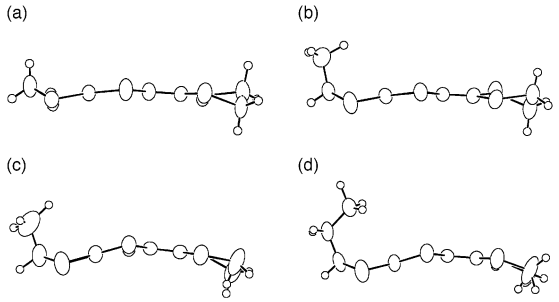

Figure 35. Side views of the molecular structures of MDHT (a), Me-MDHT in a needlelike crystal (b), Me-MDHT in a prismatic crystal (c), and Et-MDHT (d).

crystal, the methyl group of Me-MDHT is bonded to the MDHT moiety in an axial-like manner (Figure 35b) but no significant difference could be discerned between the structures of the MDHT moiety and the prototype MDHT molecule. On the other hand, the MDHT moiety of Me-MDHT in a prismatic crystal is curved toward the opposite side of the methyl group (Figure 35c). A similar curved MDHT moiety was found in the molecular structure of Et-MDHT (Figure 35d), wherein the ethyl group and the MDHT moiety overlap each other.

The CV measurements of Me-MDHT and Et-MDHT in PhCN indicated that introduction of the methyl and ethyl groups does not remarkably affect both the electron-donating ability and the on-site Coulombic repulsion of the parent MDHT molecule [MDHT, $E_1 = +0.57$, ΔE ($E_2 - E_1$) = 0.43 V (vs SCE in PhCN); Me-MDHT, $E_1 = +0.59$, ΔE ($E_2 - E_1$) = 0.40 V; Et-MDHT, $E_1 = +0.57$, ΔE ($E_2 - E_1$) = 0.41 V]. However, our attempt to prepare the Et-MDHT salts with various anions in different solvents was unsuccessful. On the other hand, single crystals of the AuI_2 salt of Me-MDHT could be obtained, although Me-MDHT with I_3^-, BF_4^-, ClO_4^-, PF_6^-, and AsF_6^- anions gave no or only a trace amount of CT salt.

The stoichiometry and structure of the AuI_2 salt of Me-MDHT was determined by X-ray analysis. The salt has a 3:1 (donor:anion) stoichiometry and consists of donor layers alternating with anion layers (Figure 36a). In the donor layer there is a monomer (corresponding to molecule A in Figure 36b) surrounded by four dimers, and the monomer has considerable positional disorder in the carbon atom

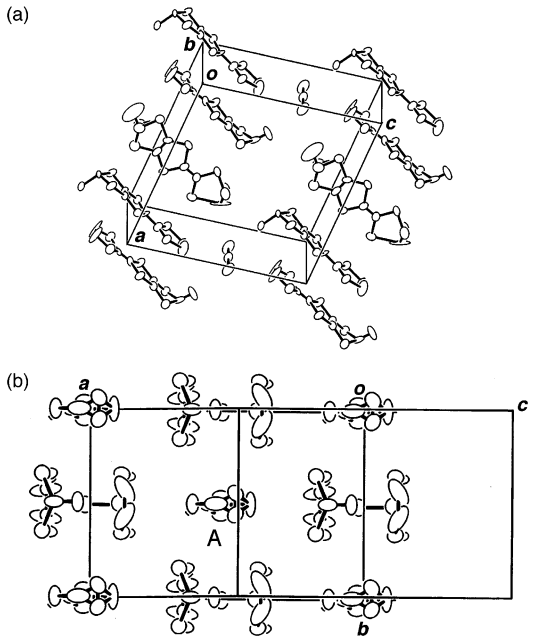

Figure 36. (a) Crystal structure of $(Me\text{-}MDHT)_3AuI_2$. (b) Donor arrangement in $(Me\text{-}MDHT)_3AuI_2$.

linking the methyl group. It is expected that charge separation among donor molecules may occur in such a donor layer containing orthogonal monomers and dimers.[49] However, an accurate estimate of the bond lengths of each donor molecule could not be carried out due to the observed disorder. The temperature dependence of the resistivity of $(Me\text{-}MDHT)_3AuI_2$ showed semiconducting behavior ($E_a = 28$ meV, $\sigma_{rt} = 8.5$ S cm^{-1}), and a significant change in the conducting behavior has not yet been observed at pressures of up to 5 kbar.

Consequently, it was found that attachment of an alkyl group, which is less bulky than a dioxane ring, to the MDHT molecule hinders a facile formation of crystalline CT salts, despite the fact that Me-MDHT and Et-MDHT have lower E_1 values than that of DODHT (+0.64 V vs SCE in PhCN). This result suggests that the *cis*-fused dioxane ring plays a critical role in crystallization of CT materials, which cannot be expected from only the electron-donating ability.

4.2. DHTTF-Fused Donors and Their Analogues

One attractive π-electron donor, formed by extending the π-system as well as containing multiple sulfur atoms, is the bis-fused TTF molecule, viz., BDT-TTP (Figure 37), which was initially proposed by Schumaker.[50] The synthetic study of BDT-TTP and its analogues by Misaki and co-workers allowed the production of a wide variety of TTF-fused donors, and many of their CT materials exhibited metallic behavior down to low temperatures.[51] Furthermore, a vinylogous bis-fused TTF, DTEDT, yielded a super-

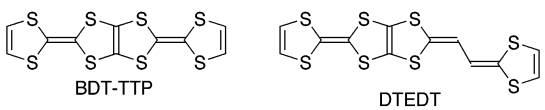

Figure 37.

conductor $(DTEDT)_3Au(CN)_2$ with a superconducting transition temperature (T_c) of 4 K.[52] The partial reduction of the π-system in BDT-TTP leads, for example, to the DHTTF-fused donor DTDH-TTP (Figure 3). It is therefore interesting to reveal whether the DTDH-TTP-type π-donors provide organic metals and superconductors. In this section, the results obtained from our studies of the fused DHTTF-TTF donors and related donors are summarized.

Single crystals of the AuI_2 (σ_{rt} = 450 S cm^{-1}),[15] BF_4 (σ_{rt} = 123 S cm^{-1}),[53] ReO_4 (σ_{rt} = 21 S cm^{-1}),[53] AsF_6 (σ_{rt} = 11 S cm^{-1}),[53] and SbF_6 (σ_{rt} = 29 S cm^{-1})[53] salts of the parent DTDH-TTP donor retained the metallic state down to 4.2 (liquid He temperature) or ca. 2 K. Interestingly, recent investigation of the DTDH-TTP salt with the paramagnetic metal complex anion $Cr(isoq)_2(NCS)_4^-$ (isoq = isoquinoline) demonstrated that (DTDH-TTP)$[Cr(isoq)_2(NCS)_4]$ exhibits bulk canted weak ferromagnetism below the critical temperature of 8.7 K.[54] The ethylenedithio-substituted derivative EDDH-TTP (Figure 3) with linear anions [I_3^- (σ_{rt} = 83 S cm^{-1}), $Au(CN)_2^-$ (σ_{rt} = 60 S cm^{-1}), and AuI_2^- (σ_{rt} = 14 S cm^{-1})] and octahedral anions [PF_6^- (σ_{rt} = 58 S cm^{-1}), AsF_6^- (σ_{rt} = 170 S cm^{-1}), and SbF_6^- (σ_{rt} = 39 S cm^{-1})] formed metallic salts down to low temperatures (4.2 or ca. 2 K).[6b,15] While the tetrahedral anion BF_4^- gave a semiconductive EDDH-TTP salt (σ_{rt} = 3.9 S cm^{-1}, E_a = 26 meV), the BF_4 salt derived from the oxygen-containing analogue of EDDH-TTP, EDOT-TTP (Figure 3), was metallic down to 1.5 K.[10e] However, the EDOT-TTP salts with other anions such as I_3^-, AuI_2^-, ClO_4^-, PF_6^-, and AsF_6^- (σ_{rt} = 10^{-1} to 10^2 S cm^{-1}) exhibited semiconducting behavior (E_a = 37−72 meV) for compressed pellets or single crystals.

The crystal structure of $(DTDH\text{-}TTP)_2SbF_6$ was determined by X-ray analysis.[53] The salt contains layers of DTDH-TTP donor molecules alternating along the c-axis with anion layers (Figure 38a). In the donor layer, DTDH-TTP molecules are slightly dimerized with interplanar distances of 3.51 and 3.54 Å to form the β-type packing motif. Short intrastack S···S contacts are observed within a donor pair with an interplanar spacing of 3.54 Å, and each donor molecule is connected by several short interstack S···S contacts (Figure 38b). The overlap integral ratio of $b1$ to $b2$ is almost equal to 1.0, substantiating a considerably uniform donor stack as a β-type salt. The tight-binding band calculation leads to the 2D band dispersion and closed Fermi surface peculiar to β-type conductors (Figure 39).

On the other hand, $(EDDH\text{-}TTP)_2X$ (X = AuI_2 and AsF_6) were found to have the κ-type donor packing motifs.[6b,15] Figure 40 shows the donor arrangement in the AuI_2 salt. The interplanar distance within a pair of donor molecules is 3.41 Å, and the dihedral angle of the molecular planes between pairs is 80.7°. These values are similar to those in κ-$(ET)_2Cu(NCS)_2$ (3.38 Å, 88°).[55] Each donor molecule is linked by several short intrapair and interpair S···S contacts, which would be responsible for the metallic behavior of this salt down to a low temperature. Unlike the AuI_2 salt, the unit cell of the AsF_6 salt contains two kinds of κ-type donor layers; however, the donor

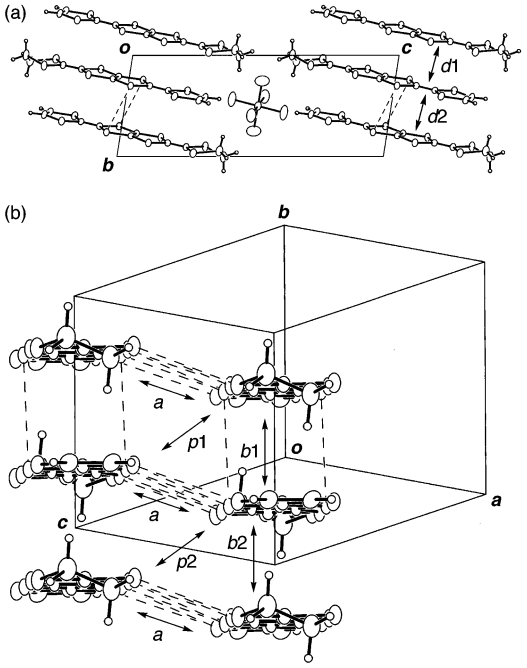

Figure 38. (a) Crystal structure of $(DTDH\text{-}TTP)_2SbF_6$ viewed along the a-axis. Short S···S contacts are drawn by broken lines. Interplanar distances in the DTDH-TTP column are 3.51 ($d1$) and 3.54 ($d2$) Å. (b) Donor arrangement in $(DTDH\text{-}TTP)_2SbF_6$. Short S···S contacts are drawn by broken lines. Intermolecular overlap integrals ($\times 10^{-3}$) $b1$, $b2$, a, $p1$, and $p2$ are 21.0, 20.8, 0.86, 9.45, and 7.41, respectively.

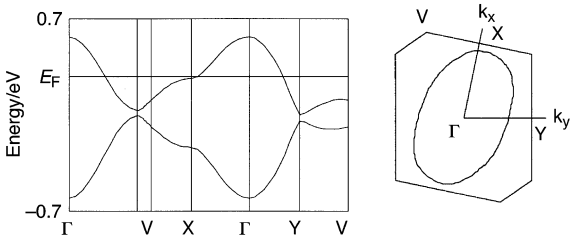

Figure 39. Energy band structure and Fermi surface of $(DTDH\text{-}TTP)_2SbF_6$.

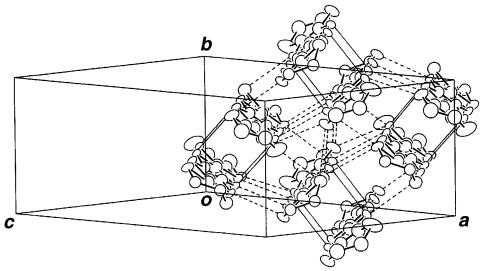

Figure 40. Donor arrangement in $(EDDH\text{-}TTP)_2AuI_2$. Short interpair S···S contacts are shown by broken lines, whereas thin lines indicate short intrapair S···S contacts. (Reprinted with permission from ref 15. Copyright 1996, The Royal Society of Chemistry.)

packing patterns in these κ-type layers are very similar to each other. In addition, the κ-type packing motif of EDDH-TTP molecules can be found in $(EDDH\text{-}TTP)_3[Cr(phen)(NCS)_4]\cdot 2CH_2Cl_2$ (phen = 1,10-phenanthroline),[49] which exhibited metallic conductivity (σ_{rt} = 100 S cm^{-1}) down to 30−50 K depending on the samples used for the conductivity measurements and obeyed the Curie−Weiss law with a Curie

constant (C) of 2.125 emu K mol^{-1} and a Weiss constant (θ) of -0.87 K. The deviation of C from the spin-only value of the Cr^{3+} ion (1.875 emu K mol^{-1}) would be attributed to the weighting error of the small amount of the sample (0.67 mg).

The above results indicate that insertion of a tetrathiapentalene (TTP) unit into the central C=C double bond of the DHTTF-type donor is a most promising molecular design for constructing π-donors leading to organic metals. Also, this architecture was found to be applicable to the dithiane analogue of EDHT, EDDT (Figure 2). That is, EDDT failed to form CT salts with the anions we examined, whereas EDDT-TTP (Figure 3), in which the TTP unit is introduced into the central C=C bond of EDDT, with AuI_2^- ($\sigma_{rt} = 36$ S cm^{-1}), BF_4^- ($\sigma_{rt} = 52$ S cm^{-1}), ClO_4^- ($\sigma_{rt} = 21$ S cm^{-1}), PF_6^- ($\sigma_{rt} = 44$ S cm^{-1}), and AsF_6^- ($\sigma_{rt} = 12$ S cm^{-1}) anions gave metallic salts, although all the variable-temperature resistivity measurements were taken on compressed pellets.[56] However, a fruitful result regarding the development of new superconductors has not yet been obtained from the studies of DTDH-TTP and its analogues.

5. New Donor Family—BDY Donors

Our studies on the production of organic metals and superconductors from DHTTF donors are directed toward the post-TTF era, and their results demonstrate that the DT unit alone is a sufficient π-system to form CT salts exhibiting metallic conductivity and superconductivity. This demonstration coupled with the finding that the fused DHTTF-TTF donors comprising three DT units, such as DTDH-TTP and EDDH-TTP (Figure 3), produce stable metallic salts with various anions encouraged development of a new donor family containing two DT units other than TTF donors. To this end, we realized, at the outset, the need to design a basic π-system in which the linkage pattern of two DT units is different from that in the TTF unit. The obvious candidate in this regard is the BDY unit (Figure 1), and our ongoing work is aimed at synthesizing a variety of BDY donors. From the BDY donors so far synthesized,[57] emphasis throughout this section will placed on studies of symmetrical BDY donors BDH-TTP (Figure 41)[57a] and BDA-TTP[57b] and unsymmetrical BDY donors DHDA-TTP[57d] and DHDE-TTP.[57e]

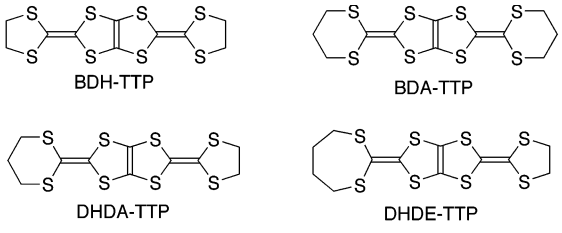

Figure 41.

5.1. Synthesis, Molecular Structures, and Electrochemical Properties

Our synthetic route to BDH-TTP and BDA-TTP involved BF_3- and Me_3Al-promoted reactions as key steps (Scheme 12). The BF_3-induced transformation

Scheme 12

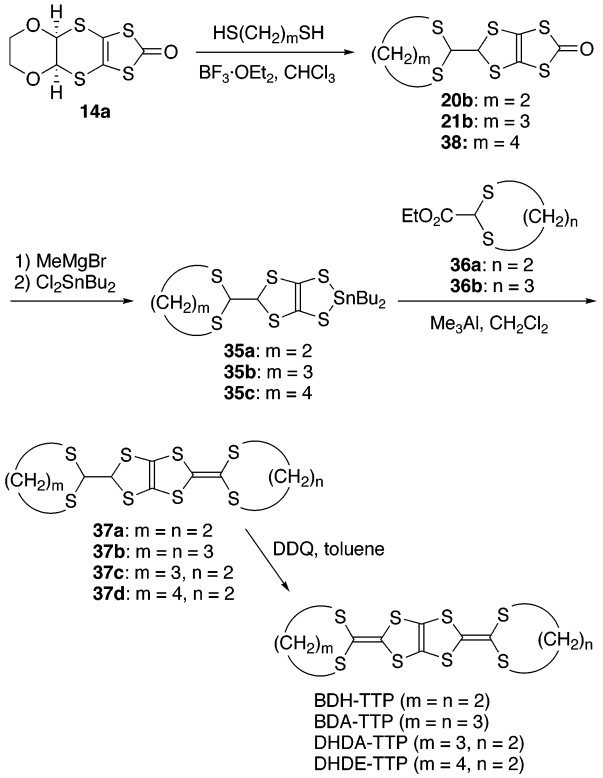

of the dioxane-fused oxone **14a** into the dithiolane- and dithiane-attached oxones **20b** and **21b** (vide supra, section 2.2) followed by sequential treatment with MeMgBr and Cl_2SnBu_2 in THF led to the corresponding labile tin dithiolates **35a**,**b**, respectively, which were immediately used for the Me_3Al-promoted coupling reactions. Reaction of **35a** with ester **36a** (2-ethoxycarbonyl-1,3-dithiolane) in the presence of Me_3Al (2 equiv) gave compound **37a** (52% overall yield from **20b**) as a precursor of BDH-TTP, and a similar reaction of **35b** with ester **36b** afforded a precursor of BDA-TTP, i.e., compound **37b** (41% overall yield from **21b**). Subsequent DDQ oxidation of **37a**,**b** in refluxing toluene furnished BDH-TTP and BDA-TTP in 89% and 80% yields, respectively. It is noteworthy that this synthetic sequence for constructing symmetrical BDY donors can be applied to synthesis of the unsymmetrical BDY donors DHDA-TTP and DHDE-TTP. The Me_3Al-promoted reaction of tin dithiolate **35b** with ester **36a** gave **37c**, which upon oxidation with DDQ in refluxing toluene led to DHDA-TTP in 85% yield. DHDE-TTP was also obtained by a five-step sequence. Thus, the $BF_3{\cdot}OEt_2$ (10 equiv) promoted reaction of **14a** with 1,4-butanedithiol gave the dithiepane-appended oxone **38** in 82% yield. Conversion of **38** into tin dithiolate **35c** under standard conditions followed by the Me_3Al (2 equiv) promoted coupling of **35c** with ester **36a** furnished **37d** (48% overall yield from **38**). Finally, DDQ oxidation of **37d** led to DHDE-TTP in 86% yield.

The molecular structures of BDH-TTP and BDA-TTP were determined by X-ray analyses. As depicted in Figure 42, the structural feature common to both molecules is that the three tetrathioethylene units are found in an almost common plane. While the two ethylene end groups of BDH-TTP are slightly dis-

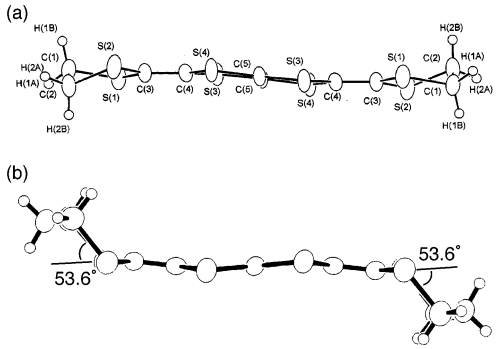

Figure 42. Side views of the molecular structures of BDH-TTP (a) (Reprinted with permission from ref 57a. Copyright 1999, Wiley-VCH.) and BDA-TTP (b).

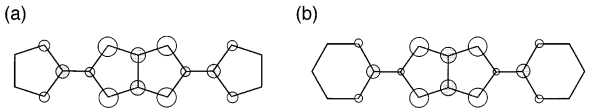

Figure 43. HOMOs of BDH-TTP (a) and BDA-TTP (b). (Reprinted with permission from ref 6d. Copyright 2004, Kodansha & Springer.)

Table 2. Oxidation Potentials of BDY Donors[a]

compound	E_1	E_2	E_3	E_4	ΔE ($E_2 - E_1$)
BDH-TTP	0.56	0.85	1.24	1.44[b]	0.29
BDA-TTP	0.67	0.90	1.31		0.23
DHDA-TTP	0.62	0.89	1.37		0.27
DHDE-TTP	0.62	0.90	1.45		0.28

[a] V vs SCE; 0.1 M n-Bu_4NClO_4 in PhCN; Pt electrode; at room temperature; under nitrogen; scan rate 50 mV s^{-1}. [b] Irreversible wave.

torted from the common plane (Figure 42a), the BDH-TTP molecule has a flatter structure compared to its structural isomer ET.[31] On the other hand, the two trimethylene end groups of BDA-TTP are far out of the common plane in opposite directions (Figure 42b), and the dihedral angle around the intramolecular sulfur-to-sulfur axis in each dithiane ring is 53.6°. Therefore, the two dithiane rings with an equivalent chair conformation cause the entire molecular structure of BDA-TTP to be less planar than that of BDH-TTP. Figure 43 shows the HOMOs of BDH-TTP and BDA-TTP calculated at the ab initio level (RHF/6-31G**).[6d] The geometries are taken from their molecular structures determined by X-ray analyses. In both HOMOs the atomic orbital coefficients of two carbon atoms on the double bond situated on the outside of the central TTP moiety differ, and the difference between these two coefficients in the HOMO of BDA-TTP is somewhat larger than that in the HOMO of BDH-TTP. Additionally, the HOMO of BDA-TTP has relatively small contributions from two sulfur atoms on the outer dithiane ring in comparison with those on the outer dithiolane ring to the HOMO of BDH-TTP.

The CV of BDH-TTP in PhCN showed three reversible oxidation waves and an additional irreversible one, whereas the CVs of BDA-TTP, DHDA-TTP, and DHDE-TTP measured under identical conditions consisted of three reversible oxidation waves. Table 2 summarizes their oxidation potentials. A comparison of the values observed for the oxidation potentials of BDH-TTP and BDA-TTP indicates that by replacing the two outer dithiolane rings of BDH-TTP with dithiane rings, the E_1 value is shifted to a more positive value and the ΔE ($E_2 - E_1$) value is smaller, suggesting that the electron-donating ability is decreased but the dicationic state is more easily generated. A similar electrochemical tendency can be found between the heterocycle-fused DHTTF donors and their dithiane analogues.[6a] It is therefore assumed that in these donor systems the dithiane ring being less planar than the dithiolane ring does not favor the conformational change into the flatter structures required to generate the cation−radical species ($D^{\bullet+}$) but once these species are formed the trimethylene end group acts as a stronger electron-donating group than the ethylene end group to lead more readily to the dication species (D^{2+}). The E_1 and ΔE ($E_2 - E_1$) values of DHDA-TTP, a hybrid of BDH-TTP and BDA-TTP, are midway between the corresponding values of BDH-TTP and BDA-TTP. These values are comparable to those of DHDE-TTP, indicating that replacement of the outer dithiane ring in DHDA-TTP with a dithiepane ring does not alter the electron-donating ability and the on-site Coulombic repulsion.

5.2. BDH-TTP Conductors

The conducting behavior of the CT complexes and salts based on BDH-TTP is summarized in Table 3. BDH-TTP reacted with TCNQ and its tetrafluoro analogue ($TCNQF_4$) at room temperature to form CT complexes, but their σ_{rt}'s were fairly low. On the contrary, the linear, tetrahedral, and octahedral anions we examined gave metallic BDH-TTP salts stable down to very low temperatures. On the resistive behavior of the BDH-TTP salt with the smallest anion Br^- among the anions listed in Table 3, the resistivity exhibited weak metallic temperature dependence below room temperature and a minimum (R_{min}) near 150 K, below which it increased gradually.[58] The temperature variation with the magnetic susceptibility of the metallic $FeCl_4$-containing BDH-TTP salt can be well fitted to the Curie−Weiss law, and the values of C and θ are 4.25 emu K mol^{-1} and 0.041 K, respectively.[59] The C is close to the value of 4.38 emu K mol^{-1} expected for a high-spin Fe^{3+} ion

Table 3. Conducting Behavior of the BDH-TTP-Based CT Materials

acceptor	D:A[a]	σ_{rt}[b]/(S cm^{-1})
TCNQ	1:1	2.0×10^{-7} (E_a = 430 meV)
$TCNQF_4$	3:2	5.6×10^{-5} (E_a = 420 meV)[c]
Br	1:0.88[d]	98 [metallic ($R_{min} \approx$ 150 K)]
I_3	2:1	230 (metallic > 2.0 K)
AuI_2	2:1	49 (metallic > 2.0 K)
BF_4	2:1	33 (metallic > 2.0 K)
ClO_4	*e*	106 (metallic > 2.2 K)
$FeCl_4$	2:1[d]	39 (metallic > 1.5 K)
PF_6	2:1	102 (metallic > 2.1 K)
AsF_6	2:1	49 (metallic > 2.0 K)

[a] Determined by elemental analysis unless otherwise noted. [b] Room-temperature conductivity measured by a four-probe technique on a single crystal unless otherwise noted. [c] Measured on a compressed pellet. [d] Determined by X-ray analysis. [e] Not determined because this salt may explode during analysis.

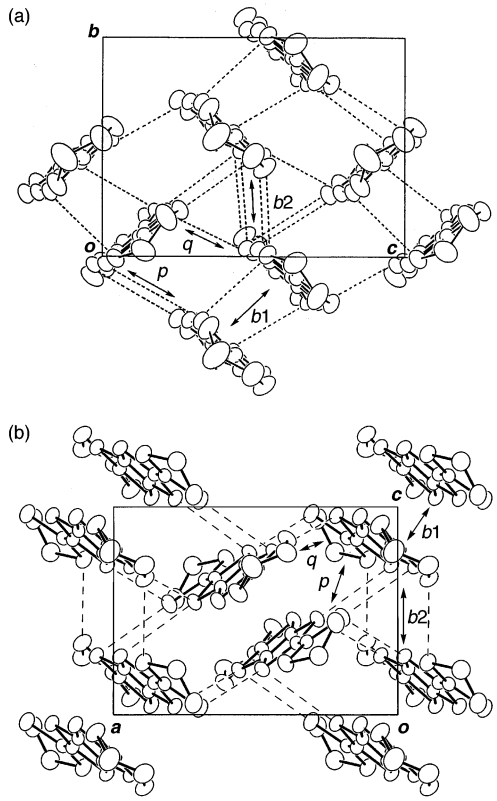

Figure 44. (a) Donor arrangement in $(BDH\text{-}TTP)_2PF_6$. Short S···S contacts are indicated by dotted lines. Intermolecular overlap integrals ($\times 10^{-3}$) $b1$, $b2$, p, and q are 20.7, 19.6, 5.9 and −7.5, respectively. (Reprinted with permission from ref 57a. Copyright 1999, Wiley-VCH.) (b) Donor arrangement in $(BDH\text{-}TTP)_2FeCl_4$. Short S···S contacts are indicated by broken lines. Intermolecular overlap integrals ($\times 10^{-3}$) $b1$, $b2$, p, and q are 19.3, 15.7, 6.39, and −6.79, respectively. (Reprinted with permission from ref 59. Copyright 2002, Elsevier.)

($S = 5/2$, $g = 2.0$), so that the Fe atom in the anion clearly dominates the measured magnetization.

X-ray analyses of $(BDH\text{-}TTP)_2X$ (X = PF_6 and $FeCl_4$) established that these salts consist of κ-type layers of BDH-TTP donor molecules alternating with anion layers.[57a,59] Between the donor layers of both salts (Figure 44) the similarities of both the interplanar distance within a donor pair (PF_6 salt, 3.53 Å; $FeCl_4$ salt, 3.59 Å) and the dihedral angle of the molecular planes between donor pairs (PF_6 salt, 82°; $FeCl_4$ salt, 83.3°) are discerned. Each donor molecule in the PF_6 salt is linked by several short intrapair and interpair S···S contacts (Figure 44a), and the large overlap integrals are also calculated within and between donor pairs, which form 2D interaction in the *bc* plane. This 2D electronic structure is responsible for the observed metallic conductivity down to low temperatures. Compared to the PF_6 salt, the donor molecule packing in the $FeCl_4$ salt seems to be somewhat loose, since there is no short intrapair S···S contact (Figure 44b). However, several short interpair S···S contacts are observed between neighboring donor molecules located out of a donor pair, and the large overlap integrals are calculated within a donor pair as well as between donor pairs, which leads to 2D interaction in the *ac* plane. On the other hand, in the $FeCl_4^-$ anion layer, consecutive anions

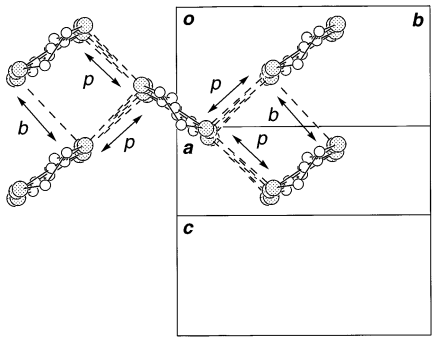

Figure 45. Donor arrangement in $(BDH\text{-}TTP)Br_{0.88}$. Short S···S contacts are drawn by broken lines. Intermolecular overlap integrals ($\times 10^{-3}$) b and p are 3.08 and 13.9, respectively. (Reprinted with permission from ref 58. Copyright 2004, EDP Sciences.)

form pairs with a Fe···Fe distance of 5.559(2) Å and the shortest Cl···Cl distance within a pair is 3.594(2) Å. The Cl···Cl distance is slightly longer than the van der Waals distance (3.50 Å), so that a superexchange mechanism would make little contribution to the magnetic behavior of the $FeCl_4$ salt. Actually, the observed θ is close to almost zero (0.041 K).

In addition to κ-type BDH-TTP salts, the θ-type BDH-TTP donor arrangement occurred in $(BDH\text{-}TTP)Br_{0.88}$ (Figure 45).[58] In the donor layer the dihedral angle between the planes formed by donor molecules on neighboring stacks is 111.3°. Several short S···S contacts are observed between stacks, and there is also one short S···S contact within a stack. This S···S contact pattern reflects the overlap integrals calculated on the donor layer, suggestive of a 2D electronic structure.

It is worth noting that similar to $(DTDH\text{-}TTP)[Cr(isoq)_2(NCS)_4]$,[54] the magnetic properties of the isomorphous $(BDH\text{-}TTP)[M(isoq)_2(NCS)_4]$ (M = Cr^{3+} and Fe^{3+}) salts were characteristic of bulk weak ferromagnets below the critical temperature of 7.6 K.[60] Furthermore, it has been reported that BDH-TTP with the photochromic nitroprusside anion $[FeNO(CN)_5]^{2-}$ yields two kinds of κ-type salts, i.e., the solvated κ-$(BDH\text{-}TTP)_4[FeNO(CN)_5]\cdot PhNO_2$ salt and κ-$(BDH\text{-}TTP)_4[FeNO(CN)_5]$, which exhibit metallic behavior down to 4.2 K.[61]

5.3. BDA-TTP Superconductors at Ambient Pressure

Before our finding of superconductivity in $(DODHT)_2X$ (X = AsF_6 and PF_6),[43a,b] we discovered a series of ambient-pressure superconductors β-$(BDA\text{-}TTP)_2X$ (X = SbF_6, AsF_6, and PF_6) which are the first organic superconductors containing no TCF unit in a donor component capable of contributing to superconductivity.[57b] The zero-field-cooled (ZFC) temperature dependence of the dc magnetization for these superconducting salts showed that the onset of diamagnetic transition occurs at a temperature of 6.9 K for the SbF_6 salt and 5.9 K for both the AsF_6 and PF_6 salts (Figure 46a). Superconductivity in the SbF_6 and AsF_6 salts was also recorded by the temperature dependence of their electrical resistivities under ambient pressure. As shown in Figure 46b, the resistivity of the SbF_6 salt ($\sigma_{rt} = 1.5$ S cm^{-1}) increased

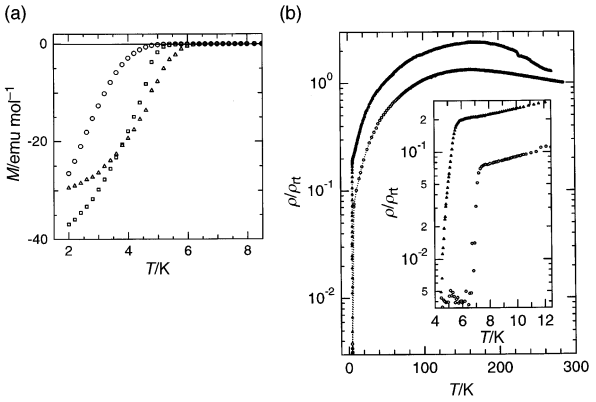

Figure 46. (a) Temperature dependence of the ZFC dc magnetization for the SbF_6 (triangles), AsF_6 (squares), and PF_6 (circles) salts of BDA-TTP under an applied magnetic field of 1 Oe. (b) Temperature dependence of the relative resistivities for the SbF_6 (circles) and AsF_6 (triangles) salts of BDA-TTP. (inset) Relative resistivities in the low-temperature region. Dotted lines are visual guides.

like that in a semiconductor on cooling from room temperature to near 150 K and then exhibited metallic behavior down to 7.5 K. Below this temperature the resistivity displayed an abrupt drop and became almost zero below 6.5 K. The onset of the superconducting transition observed in the subsequent heating process occurred at 7.5 K (inset in Figure 46b), which is slightly higher than that in the magnetization measurement. Similar resistive maximum and superconductive behavior were found in the variable-temperature resistivity measurement of the AsF_6 salt (σ_{rt} = 2.9 S cm^{-1}). Below 160 K the resistivity of this salt decreased with decreasing temperature down to a superconducting transition with onset at 5.8 K, which is comparable to that of the magnetic transition, and zero resistance was observed below 4.4 K. Although we carried out resistive measurements on numerous single crystals of the PF_6 salt (σ_{rt} = 3.8 S cm^{-1}), all crystal specimens were found to disintegrate at temperatures in the range of 110−140 K. In this temperature region, since no anomaly in the magnetic susceptibility was observed, it appears that there is no marked change in the electronic state of this salt. Decomposition of these crystal specimens could therefore be attributed to the stresses of the resistance-measuring probes or some other artifact of the measurements. Owing to the fragile nature of the crystals, the superconducting transition of the PF_6 salt could not be determined by resistive measurements. Further characterization of the (BDA-TTP)$_2$SbF$_6$ superconductor has been conducted by Ishiguro et al.[62] and, subsequently, Choi et al.[63] The most distinct feature of (BDA-TTP)$_2$SbF$_6$ is its largest value of the effective cyclotron mass (m_c* = 12.4 ± 1.1 m_e) yet found in organic superconductors.[63]

All superconductors crystallized in the triclinic space group $P\bar{1}$ and are isostructual. Figure 47 shows the crystal structure of (BDA-TTP)$_2$SbF$_6$ in which the donor molecular packing is very similar to that in β-(ET)$_2$I$_3$.[33] As shown in Figure 48, the whole molecular structure of BDA-TTP in this salt is somewhat flatter than that in the neutral state (Figure 42b). Although the chair conformations of two outer dithiane

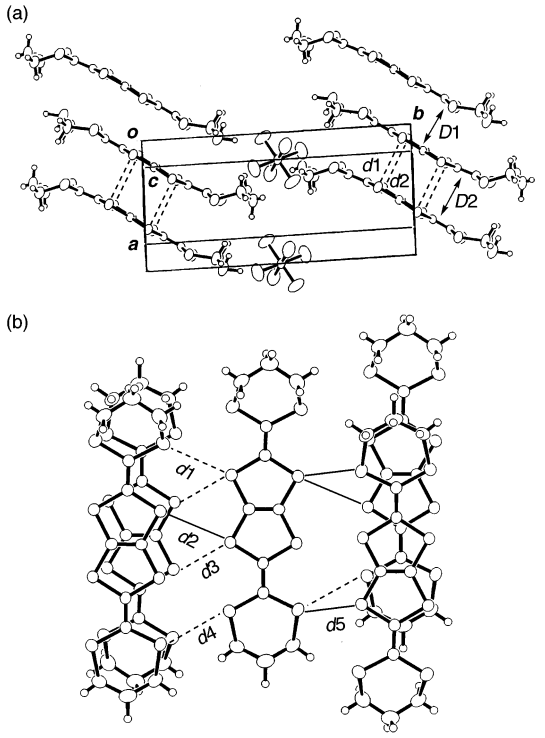

Figure 47. (a) Crystal structure of (BDA-TTP)$_2$SbF$_6$. Short S···S contacts are indicated by broken lines: $d1$ = 3.694(1), $d2$ = 3.686(1) Å. Interplanar distances in the BDA-TTP column are 3.52 ($D1$) and 3.80 ($D2$) Å. (b) Donor arrangement in (BDA-TTP)$_2$SbF$_6$. Intermolecular S···S distances close to 3.70 Å are indicated by broken lines: $d1$ = 3.722(1), $d3$ = 3.694(1), $d4$ = 3.697(1) Å. Short S···S contacts are indicated by thin lines: $d2$ = 3.645(1), $d5$ = 3.649(1) Å.

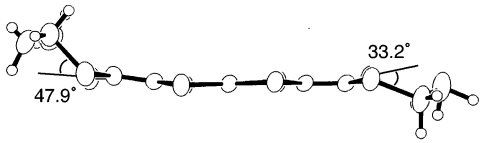

Figure 48. Molecular structure of BDA-TTP in (BDA-TTP)$_2$SbF$_6$.

rings remain unchanged, they are nonequivalent and their dihedral angles around the intramolecular sulfur-to-sulfur axis are 47.9° and 33.2°, respectively. The BDA-TTP molecules are stacked along the [101] direction and somewhat dimerized: the donor molecules alternate at interplanar distances of 3.52 and 3.80 Å (Figure 47a). The two donor molecules being 3.52 Å apart mutually shifted, while one pair with an interplanar spacing of 3.80 Å has a nearly eclipsed arrangement in which there are two S···S contacts slightly shorter than 3.70 Å. As shown in Figure 47b, three intermolecular S···S distances close to 3.70 Å and two short S···S contacts are observed between stacks. The structural characteristics of β-(BDA-TTP)$_2$SbF$_6$ also hold for the isostructural β-(BDA-TTP)$_2$X (X = AsF_6 and PF_6) superconductors.

The S···S contact pattern found in intra- and interstacks of each BDA-TTP superconductor reflects the small anisotropy of the overlap integrals in the ac plane (Figure 49). Likewise, a tight-binding band calculation for each BDA-TTP superconductor leads to the 2D band dispersion relation and nearly isotropic closed Fermi surface, which is peculiar to the

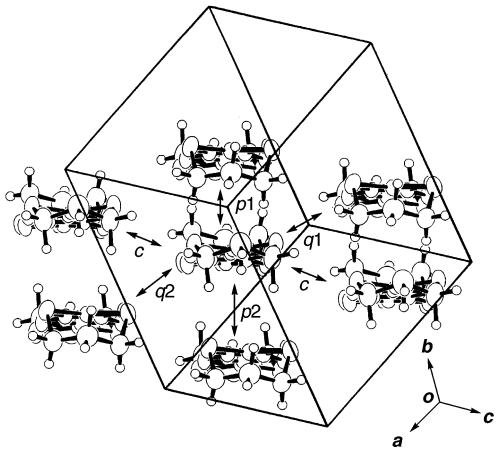

Figure 49. Values of intermolecular overlap integrals ($\times 10^{-3}$): (BDA-TTP)$_2$SbF$_6$, $c = -0.44$, $p1 = 14.7$, $p2 = 6.26$, $q1 = 8.14$, $q2 = 8.89$; (BDA-TTP)$_2$AsF$_6$, $c = 0.34$, $p1 = 14.8$, $p2 = 5.31$, $q1 = 7.59$, $q2 = 9.00$; (BDA-TTP)$_2$PF$_6$, $c = 0.41$, $p1 = 13.9$, $p2 = 9.02$, $q1 = 6.88$, $q2 = 8.63$.

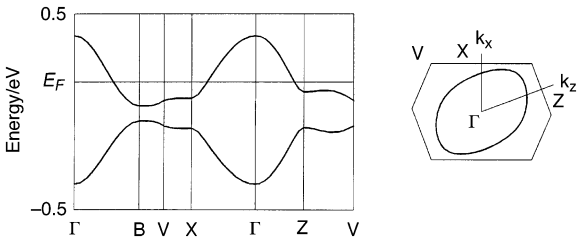

Figure 50. Energy band structure and Fermi surface of (BDA-TTP)$_2$SbF$_6$.

β-structure (for example, see Figure 50 for the SbF$_6$ salt). It should be noted that the largest overlap integrals in all three BDA-TTP superconductors (14.7, 14.8, and 13.9 $\times$ 10^{-3} for the SbF$_6$, AsF$_6$, and PF$_6$ salts, respectively) are roughly one-half those in the known organic superconductors such as β-(ET)$_2$I$_3$ (24.5×10^{-3})[33c] and κ-(ET)$_2$Cu(NCS)$_2$ (25.7×10^{-3}),[64] demonstrating that they are characterized as a superconductor system with soft (or loose) donor packing motifs.

5.4. BDA-TTP Superconductors under Applied Pressures

Following the discovery of ambient-pressure superconductors β-(BDA-TTP)$_2$X (X = SbF$_6$, AsF$_6$, and PF$_6$),[57b] we found that the GaCl$_4$ and FeCl$_4$ salts of BDA-TTP undergo superconducting transitions under applied pressures.[65]

These salts are isostructural with each other and have β-type structures. The crystal structure of β-(BDA-TTP)$_2$FeCl$_4$ was determined both at room temperature and at 95 K.[59,66] Figure 51 shows the crystal structure at room temperature. The asymmetric unit consists of one FeCl$_4^-$ anion and two crystallographically independent BDA-TTP molecules. The BDA-TTP donor molecules and the FeCl$_4^-$ anions are arranged in alternating layers along the b-axis, so that the Fe···Fe distance between the most adjacent anions along the b-axis [19.535(6) Å] is substantially longer than those along the a- and c-axes [6.227(3) and 7.731(4) Å]. At 95 K, the Fe···Fe distances along the a- and c-axes become shortened

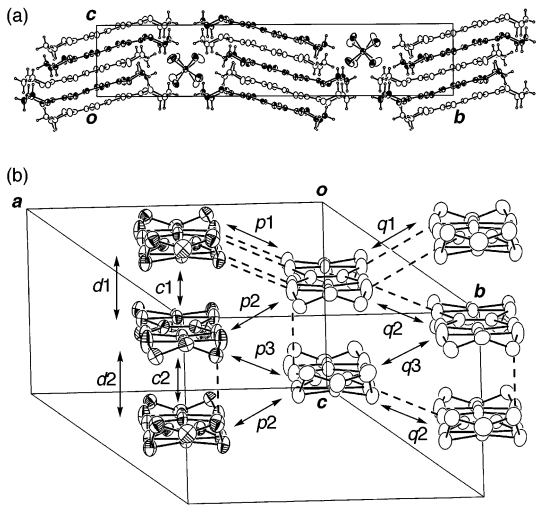

Figure 51. (a) Crystal structure of (BDA-TTP)$_2$FeCl$_4$ viewed along the a-axis; open circles indicate the back molecules. (b) Donor arrangement in (BDA-TTP)$_2$FeCl$_4$. Interplanar distances in the BDA-TTP column are 3.56 ($d1$) and 3.89 ($d2$) Å. Short S···S contacts are drawn by broken lines. Intermolecular overlap integrals ($\times 10^{-3}$) $c1$, $c2$, $p1$, $p2$, $p3$, $q1$, $q2$, and $q3$ are 14.4, 13.5, 1.88, −7.34, 3.44, 6.99, −5.62, and 5.49, respectively, whereas the corresponding values at 95 K are 15.4, 12.5, 1.49, −7.55, 3.19, 7.11, −5.65, and 5.39, respectively. (Reprinted with permission from refs 59 and 66. Copyright 2002 and 2001, respectively, The Royal Society of Chemistry and Elsevier.)

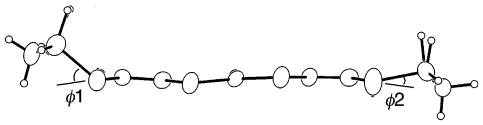

Figure 52. Molecular structure of one BDA-TTP molecule in (BDA-TTP)$_2$FeCl$_4$. The dihedral angles $\phi1$ and $\phi2$ are 38.6° and 13.0°, whereas the corresponding angles in the other BDA-TTP are 39.1° and 13.0°. (Reprinted with permission from refs 59 and 66. Copyright 2002 and 2001, respectively, The Royal Society of Chemistry and Elsevier.)

to 6.192(2) and 7.580(2) Å, respectively. At room temperature, two independent BDA-TTP molecules have similar molecular structures, in both of which the two outer dithiane rings adopt nonequivalent chair conformations: their respective dihedral angles around the intramolecular sulfur-to-sulfur axis in one BDA-TTP molecule are 38.6° and 13.0°, and the corresponding angles in the other are 39.1° and 13.0° (Figure 52). Thus, one dithiane ring of each independent BDA-TTP molecule is much flatter than that of each BDA-TTP molecule in the superconductors β-(BDA-TTP)$_2$X (X = SbF$_6$, AsF$_6$, and PF$_6$) (Figure 48). Another point worth noting is that the two trimethylene end groups of each independent BDA-TTP molecule are found on the same side of the molecular plane, which is in contrast to the fact that those of the BDA-TTP molecules in both the neutral state and the superconducting salts appear with opposite orientation with respect to the molecular plane (Figures 42b and 48). The BDA-TTP molecules form slipped stacks along the c-axis with some dimerization (interplanar distances of 3.56 and 3.89 Å) so as to minimize the steric hindrance of the less flat dithiane ring. There is only one short S···S contact within the stack, whereas several short S···S

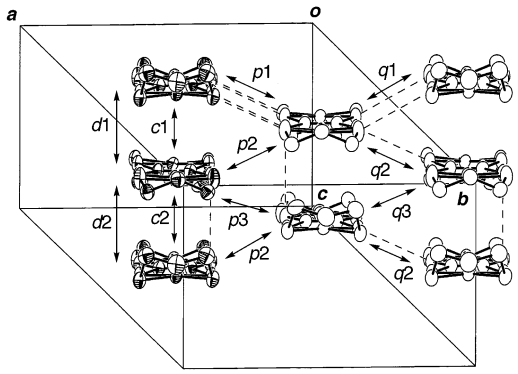

Figure 53. Donor arrangement in $(BDA\text{-}TTP)_2GaCl_4$. Interplanar distances in the BDA-TTP column are 3.56 ($d1$) and 3.90 ($d2$) Å. Short S···S contacts are drawn by broken lines. Intermolecular overlap integrals ($\times 10^{-3}$) $c1$, $c2$, $p1$, $p2$, $p3$, $q1$, $q2$, and $q3$ are 14.8, 13.4, 2.40, −7.03, 3.05, 6.92, −5.30, and 5.48, respectively. (Reprinted with permission from ref 65a. Copyright 2003, The Royal Society of Chemistry.)

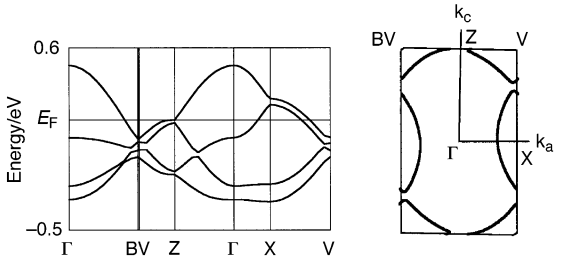

Figure 54. Energy band structure and Fermi surface of $(BDA\text{-}TTP)_2FeCl_4$. (Reprinted with permission from ref 58. Copyright 2004, EDP Sciences.)

contacts exist between stacks (Figure 51b). At 95 K, although the interplanar distances in the stack are shortened to 3.47 and 3.84 Å, the number of short S···S contacts does not increase. The S···S contact pattern observed at room temperature, however, does not always reflect the magnitude of the overlap integrals calculated on the donor layer.[47] The largest overlap integral (14.4×10^{-3}) is almost equal to those found in the BDA-TTP superconductors, suggesting that the BDA-TTP molecules in this salt are also packed loosely. The "softness" of the donor molecule packing remains almost unchanged at 95 K, as can be seen from the values of the overlap integrals given in the legend to Figure 51b. Moreover, even at 95 K the conformations of two independent BDA-TTP molecules are analogous to those found at room temperature.

The donor arrangement of β-$(BDA\text{-}TTP)_2GaCl_4$ is shown in Figure 53.[65a] No significant differences of both the pattern of short S···S contacts and the values of the overlap integrals could be discerned between the donor layers of the $GaCl_4$ and $FeCl_4$ salts. It is not surprising, therefore, that the band structures and Fermi surfaces of both salts are almost the same (for example, see Figure 54 for the $FeCl_4$ salt).[58] These Fermi surfaces are similar to that of κ-$(ET)_2Cu(NCS)_2$[64] except for a slight deviation of the degeneracy on the X−V zone boundary, which originates in the presence of two crystallographically independent donor molecules and leads to open and closed hole-like orbital sections.

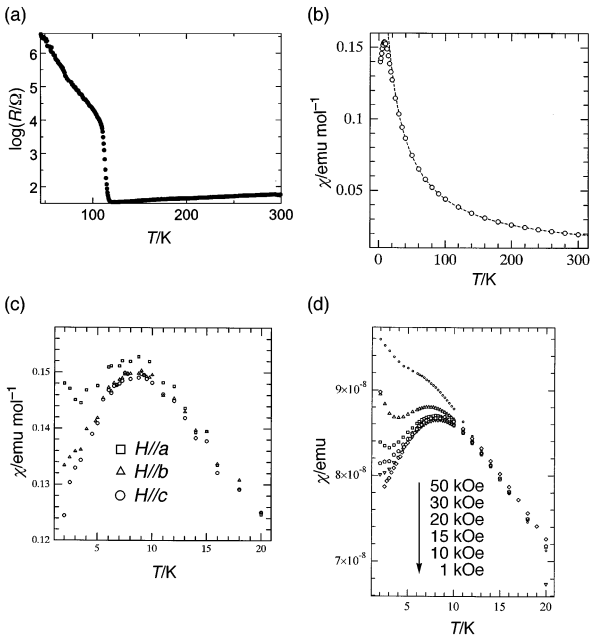

Figure 55. (a) Temperature dependence of the resistance of $(BDA\text{-}TTP)_2FeCl_4$. (Reprinted with permission from refs 59 and 66. Copyright 2002 and 2001, respectively, The Royal Society of Chemistry and Elsevier.) (b) Temperature dependence of the susceptibility of $(BDA\text{-}TTP)_2FeCl_4$. The dotted line is a Curie−Weiss fit (see text). (Reprinted with permission from refs 59 and 66. Copyright 2002 and 2001, respectively, The Royal Society of Chemistry and Elsevier.) (c) Magnetic anisotropy of $(BDA\text{-}TTP)_2FeCl_4$ in magnetic fields approximately parallel to the a-, b-, and c-axes ($H//a$, $H//b$, and $H//c$). (Reprinted with permission from refs 59 and 66. Copyright 2002 and 2001, respectively, The Royal Society of Chemistry and Elsevier.) (d) Magnetic field dependence of the susceptibility of $(BDA\text{-}TTP)_2FeCl_4$. (Reprinted with permission from ref 59. Copyright 2002, Elsevier.)

The resistivity of β-$(BDA\text{-}TTP)_2FeCl_4$ as a function of temperature showed that the salt ($\sigma_{rt} = 9.4$ S cm^{-1}) is metallic down to 113 K, at which temperature it undergoes a sharp MI transition (Figure 55a). As a cause of this MI transition, we first anticipated charge separation between two independent donors in the stack.[66] However, no appreciable conformational change in the donor molecules occurs at 95 K, so the reason for this MI transition has not yet been elucidated. Figure 55b shows the temperature dependence of the magnetic susceptibility of this salt from 300 to 2 K. The susceptibility obeys the Curie−Weiss law ($C = 4.48$ emu K mol^{-1}, $\theta = -15.1$ K) over the entire temperature range 40−300 K. From the C close to the value (4.38 emu K mol^{-1}) predicted for a high-spin Fe^{3+} ion, it is expected that the magnetic properties of this salt are dominated by the anions. Below 40 K, the susceptibility increased to a maximum near 8.5 K, after which it decreased rapidly. As shown in Figure 55c, the susceptibilities, which were measured under the magnetic fields applied along the directions approximately parallel to the crystallographic a-, b-, and c-axes, were anisotropic below ca. 8.5 K, substantiating antiferromagnetic ordering with the Néel temperature (T_N) of ca. 8.5 K. Below T_N, the easy spin axis seems to lie close to the intrastacking c-direction of the donor molecules. Accordingly, considering that the shortest Fe···Fe

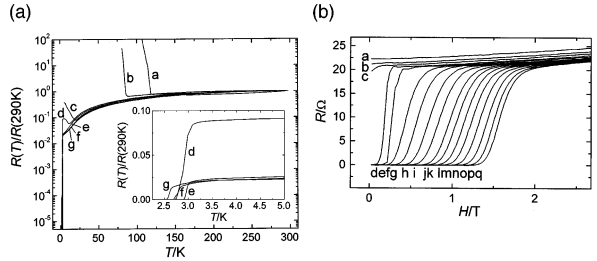

Figure 56. (a) Temperature dependence of the relative resistances for $(BDA\text{-}TTP)_2GaCl_4$ at 0 (a), 2.8 (b), 5.7 (c), 7.6 (d), 8.3 (e), 9.0 (f), and 9.7 (g) kbar. (inset) Relative resistances in the low-temperature region. (b) MRs of $(BDA\text{-}TTP)_2GaCl_4$ under 8.3 kbar at 4.2 (a), 3.5 (b), 3.0 (c), 2.5 (d), 2.2 (e), 1.9 (f), 1.7 (g), 1.5 (h), 1.3 (i), 1.2 (j), 1.1 (k), 1.0 (l), 0.9 (m), 0.8 (n), 0.7 (o), 0.6 (p), and 0.48 (q) K. (Reprinted with permission from ref 65a. Copyright 2003, The Royal Society of Chemistry.)

distance along the *c*-axis is longer than 6 Å, the donor molecules could mediate the observed antiferromagnetic order between the Fe^{3+} ions.[67] In addition, the magnetic field dependence of the susceptibility using randomly orientated multiple crystals indicated that the antiferromagnetic transition begins to disappear near 30 kOe (Figure 55d). These results demonstrate that β-$(BDA\text{-}TTP)_2FeCl_4$ is the first non-TCF-based salt in which metallic conductivity and antiferromagnetism can coexist.

Analogous to β-$(BDA\text{-}TTP)_2FeCl_4$, β-$(BDA\text{-}TTP)_2GaCl_4$ was found to exhibit a sharp MI transition at 118 K. Surprisingly, the temperature of the MI transition decreased as pressure was increased, and at 7.6 kbar, a trace of the MI transition followed by an abrupt drop in resistivity attributable to a superconducting transition with an onset of 3.1 K were observed (Figure 56a).[65a] With further increases in the pressure up to 9.7 kbar, the MI transition was completely suppressed but the superconducting transition still remained, the temperature of which gradually decreased at 9.0 and 9.7 kbar, as found in most of the organic superconductors.[2] As shown in Figure 56b, the magnetoresistances (MRs) of this salt measured at various temperatures under an applied pressure of 8.3 kbar clearly indicated that the resistivities at all temperatures below 3.0 K were restored by increasing magnetic field, which adds to the superconductivity of this salt. A similar pressure-induced suppression of an MI transition and subsequent appearance of a superconducting state could be observed in β-$(BDA\text{-}TTP)_2FeCl_4$ (Figure 57).[65b,c] The variable-temperature MR measurements of this salt at 9.7 kbar provide evidence for superconductivity (inset in Figure 57). Figure 58 shows the pressure−temperature ($P-T$) phase diagrams of β-$(BDA\text{-}TTP)_2X$ (X = $FeCl_4$ and $GaCl_4$), which are very similar to each other, although T_c (~2 K) of the $FeCl_4$ salt is lower than that (~3 K) of the $GaCl_4$ salt.

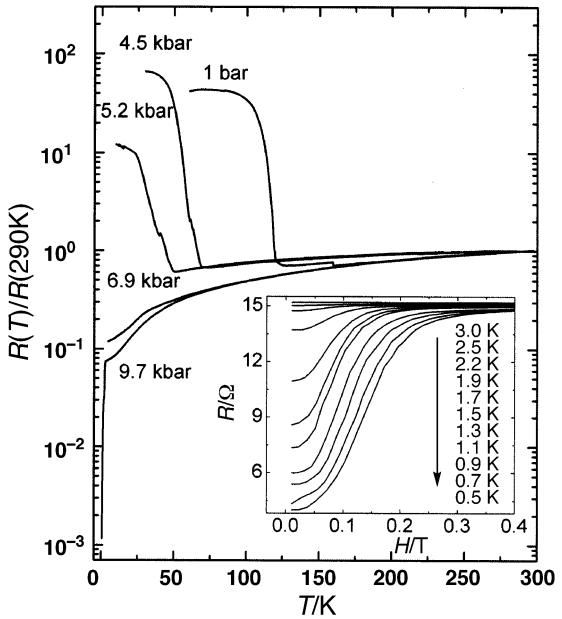

Figure 57. Temperature dependence of the relative resistances for $(BDA\text{-}TTP)_2FeCl_4$ at different pressures. (inset) MRs of $(BDA\text{-}TTP)_2FeCl_4$ at various temperatures under 9.7 kbar.

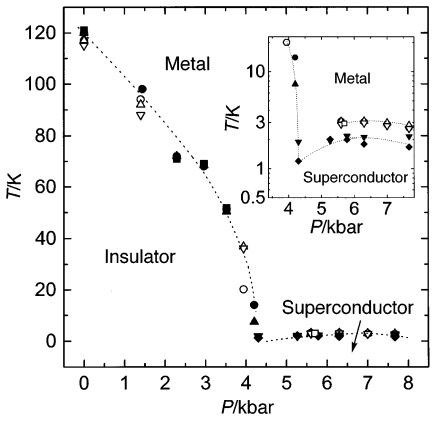

Figure 58. $P-T$ phase diagrams of $(BDA\text{-}TTP)_2X$ (X = $GaCl_4$ and $FeCl_4$). Open and solid symbols are for the $GaCl_4$ and $FeCl_4$ salts, respectively. Different symbols indicate different samples. Dotted lines are visual guides. (Reprinted with permission from ref 6e. Copyright 2004, The Royal Society of Chemistry.)

5.5. Other BDA-TTP Conductors

In contrast to the formation of the TCNQ complex with BDH-TTP at room temperature, BDA-TTP yielded no crystalline CT complex with TCNQ at room temperature, probably due to its higher E_1 value relative to that of BDH-TTP (Table 2). Heating was thus necessitated to obtain the TCNQ complex with BDA-TTP, whereas BDA-TTP with a stronger acceptor, $TCNQF_4$, formed the CT complex at room temperature. The resulting TCNQ and $TCNQF_4$ complexes showed low σ_{rt}'s (Table 4), which are not superior to those of the corresponding complexes with BDH-TTP. As for the conducting behavior of the BDA-TTP salts with the linear and tetrahedral anions so far examined,[57b,58,68] the I_3, BF_4, and ClO_4 salts exhibited semiconductive behavior. On the other hand, the resistivity of the $BF_4 \cdot H_2O$ hydrate showed weak metallic behavior around room temperature, and the $ClO_4 \cdot H_2O$ hydrate was a small gap semiconductor. The conducting behavior of the solvated $(BDA\text{-}TTP)_3X \cdot PhCl$ (X = $GaCl_4$ and $FeCl_4$) salts, which were concomitantly obtained when β-$(BDA\text{-}TTP)_2X$ (X = $GaCl_4$ and $FeCl_4$) were prepared by electrocrystallization in 5% EtOH−PhCl,[65a,59,66] was

Table 4. Conducting Behavior of the BDA-TTP-Based CT Materials

acceptor	D:A	σ_{rt}[a]/(S cm^{-1})
TCNQ	2:1[b]	$<10^{-6}$
$TCNQF_4$	1:1[b]	1.2×10^{-5} [c]
I_3	2:1[b]	18 (E_a = 54 meV)[d]
BF_4	2:1[e]	19 (E_a = 25 meV)
$BF_4 \cdot H_2O$	2:1[e]	3.3 (metallic-like $\approx$ rt[f])
ClO_4	2:1[e]	7.2×10^{-1} (E_a = 45 meV)
$ClO_4 \cdot H_2O$	2:1[e]	2.4 (E_a = 3 meV)
$GaCl_4 \cdot PhCl$	3:1[e]	3.3×10^{-3} (E_a = 150 meV)
$FeCl_4 \cdot PhCl$	3:1[e]	2.0×10^{-2} (E_a = 110 meV)
$ReO_4 \cdot PhCl$	3:1[e]	150 (E_a = 120 meV)

[a] Room-temperature conductivity measured by a four-probe technique on a single crystal unless otherwise noted. [b] Determined by elemental analysis. [c] Measured on a compressed pellet. [d] The revised data by reexamination, see ref 57b for the original data. [e] Determined by X-ray analysis. [f] Room temperature.

semiconductive. The $FeCl_4 \cdot PhCl$ salt behaved as a Curie−Weiss paramagnet with fitted C = 4.42 emu K mol^{-1} and $\theta = -0.35$ K, and the small negative θ signifies very weak antiferromagnetic interaction between the Fe moments. The solvated $(BDA\text{-}TTP)_3ReO_4 \cdot PhCl$ salt showed a high σ_{rt}, but the temperature dependence of its resistivity exhibited semiconductive behavior.

5.6. DHDA-TTP and DHDE-TTP Conductors

Similar to BDH-TTP, DHDA-TTP reacted with TCNQ and $TCNQF_4$ at room temperature to give CT complexes whose σ_{rt}'s were, however, very low (Table 5).[57d] In contrast, the DHDA-TTP salts with linear anions and a relatively small tetrahedral anion, such as I_3^-, AuI_2^-, and BF_4^-, remained metallic down to 2 K. Among these, the AuI_2 salt was found to have the κ-type structure with a 4:1 (donor:anion) stoichiometry by X-ray analysis. Additionally, the larger tetrahedral ClO_4^- anion and the octahedral PF_6^- and AsF_6^- anions led to metallic DHDA-TTP salts, which underwent MI transitions near 80, 30, and 60 K, respectively. X-ray analyses of these salts revealed that they are all β-type salts and isostructural. On the other hand, the larger octahedral SbF_6^- anion formed a semiconductive DHDA-TTP salt with a small E_a of 16 meV, a preliminary X-ray analysis of which suggested that the salt has a κ-type donor packing motif.

Table 5. Conducting Behavior of the DHDA-TTP-Based CT Materials

acceptor	D:A[a]	σ_{rt}[b]/(S cm^{-1})
TCNQ	3:1	$<10^{-6}$ [c]
$TCNQF_4$	3:1	$<10^{-6}$ [c]
I_3	3:1	53 (metallic > 2 K)
AuI_2	4:1[d]	7.4 (metallic > 2 K)
BF_4	2:1	2.3 (metallic > 2 K)
ClO_4	2:1[d]	9.1 (T_{MI}[e] $\approx$ 80 K)
PF_6	2:1	8.1 (T_{MI}[e] $\approx$ 30 K)
AsF_6	2:1	39 (T_{MI}[e] $\approx$ 60 K)
SbF_6	2:1[d]	2.6 (E_a = 16 meV)

[a] Determined by elemental analysis unless otherwise noted. [b] Room-temperature conductivity measured by a four-probe technique on a single crystal unless otherwise noted. [c] Measured on a compressed pellet. [d] Determined by X-ray analysis. [e] Temperature of an MI transition.

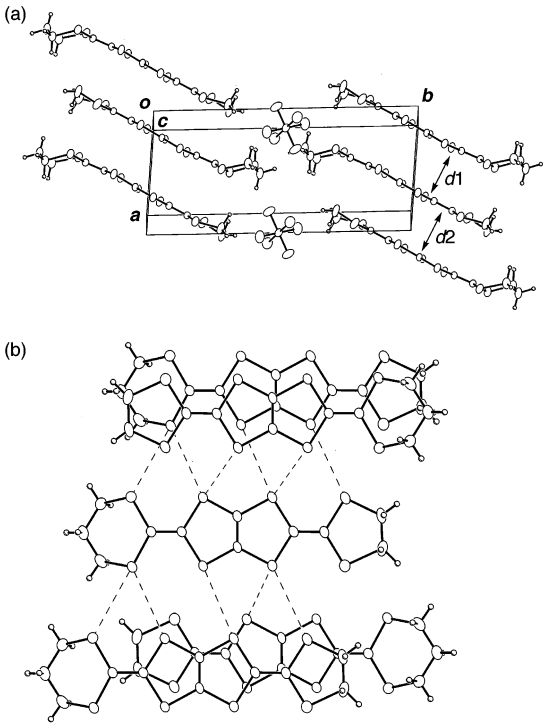

Figure 59. (a) Crystal structure of $(DHDA\text{-}TTP)_2PF_6$. Interplanar distances in the DHDA-TTP column are 3.70 ($d1$) and 3.66 ($d2$) Å. (b) Donor arrangement in $(DHDA\text{-}TTP)_2PF_6$. Short interstack S···S contacts are indicated by broken lines. (Reprinted with permission from ref 57d. Copyright 2002, The Royal Society of Chemistry.)

Figure 59a shows the crystal structure of the metallic β-$(DHDA\text{-}TTP)_2PF_6$ salt with an MI transition temperature of ca. 30 K.[57d] The donor molecular packing is similar to those of the three isomorphous superconductors β-$(BDA\text{-}TTP)_2X$ (X = SbF_6, AsF_6, and PF_6). In this salt the ethylene end group of the DHDA-TTP molecule is found essentially in the molecular plane, whereas the trimethylene end group is far out of the molecular plane. The outer dithiane ring adopts a chair conformation, and the dihedral angle around the intramolecular sulfur-to-sulfur axis is 40.6°, which is almost equal to the average value of the two corresponding dihedral angles of the BDA-TTP molecule in each BDA-TTP superconductor. The DHDA-TTP molecules are stacked along the [101] direction and slightly dimerized: the molecular planes of the donor molecules alternate at separations of 3.66 and 3.70 Å. One pair with an interplanar spacing of 3.66 Å has a slipped arrangement, while the other with an interplanar spacing of 3.70 Å has a nearly eclipsed arrangement. There are several short S···S contacts between stacks (Figure 59b), but no short S···S contact can be observed within the stack, which is in contrast to the S···S contact patterns found in the three BDA-TTP superconductors. The tight-binding band calculation results in the 2D band dispersion relation and closed Fermi surface (Figure 60). The Fermi surface of this salt is less round than those of the three BDA-TTP superconductors, suggesting the occurrence of nesting responsible for the MI transition at ca. 30 K.

The crystal structure of the 4:1 salt κ-$(DHDA\text{-}TTP)_4AuI_2$ is shown in Figure 61a.[57e] In the κ-type

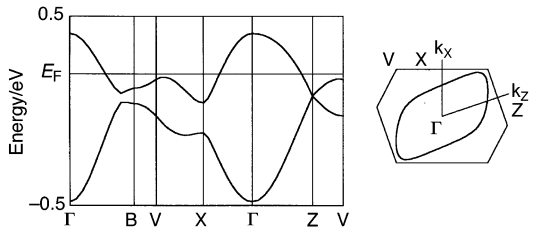

Figure 60. Energy band structure and Fermi surface of $(DHDA\text{-}TTP)_2PF_6$. (Reprinted with permission from ref 57d. Copyright 2002, The Royal Society of Chemistry.)

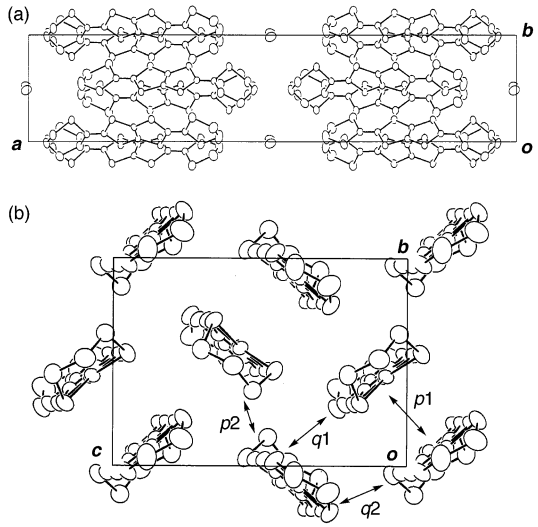

Figure 61. (a) Crystal structure of $(DHDA\text{-}TTP)_4AuI_2$ viewed along the *c*-axis. (b) Donor arrangement in $(DHDA\text{-}TTP)_4AuI_2$. Intermolecular overlap integrals ($\times 10^{-3}$) $p1$, $p2$, $q1$, and $q2$ are 12.6, 12.4, 4.46, and −2.88, respectively. (Reprinted with permission from ref 57e. Copyright 2003, Elsevier.)

donor layer (Figure 61b), the interplanar distance within a donor pair is 3.50 Å and the dihedral angle of the molecular planes between donor pairs is 80.8°. However, in contrast to κ-$(BDH\text{-}TTP)_2X$ (X = PF_6 and $FeCl_4$) (vide supra, section 5.2), no short S···S contact is observed between donor molecules. This is probably due to the steric hindrance arising from the nonplanar conformation of the outer dithiane ring. Nevertheless, the comparatively large overlap integrals are calculated between donor pairs as well as within a donor pair, which would lead to a 2D electronic structure responsible for metallic conductivity down to low temperatures.

Eventually the DHDA-TTP donor inherits, to some extent, the ability to form stable metallic CT salts from BDH-TTP. On the other hand, the octahedral PF_6^- and AsF_6^- anions, providing the isomorphous superconducting BDA-TTP salts, also give the isostructural metallic DHDA-TTP salts, which exhibit MI transitions instead of superconductivity at ambient pressure.

Another unsymmetrical BDY donor DHDE-TTP, which contains the seven- and five-membered outer rings, gave semiconducting AuI_2, BF_4, ClO_4, PF_6, and AsF_6 salts with $E_a = 53-270$ meV ($\sigma_{rt} = 10^0$ to 10^1 S cm^{-1}).[57e] On the other hand, the temperature dependence of the resistivity for the I_3 salt of DHDE-TTP ($\sigma_{rt} = 52$ S cm^{-1}) indicated that the resistivity decreases only slightly from room temperature to near 260 K, below which it increases gradually. Thus, at present, expansion of the outer ring of a BDY donor by a dithiepane ring seems to be an unfavorable structural modification to obtain stable organic metals.

6. Conclusions and Outlook

Since the discovery of the first organic superconductor $(TMTSF)_2PF_6$,[69] all organic π-donors leading to superconductors were limited to the TCF-containing compounds until recently;[70] hence, further advance in this field required extension of the scope of π-electron donors capable of producing new superconductors. Our discovery of superconductivity in a series of CT salts of DODHT and BDA-TTP presents the first step forward in that direction and demonstrates that TCF donors are no longer essential to the production of organic superconductors.

Our results obtained from studies of BDH-TTP and BDA-TTP offer the following stepwise access to achievement of organic superconductivity. First, it would be important to construct π-donor molecules that can generate tight intermolecular interaction to realize the stable metallic state, irrespective of whether they contain the TCF unit. The next step would be to clarify how structural modifications to those π-donors give rise to moderately soft donor packing motifs when the CT materials are being formed. An increase of steric bulk on the periphery of BDH-TTP by introducing trimethylene groups instead of ethylene groups provides a good example of a way to address this issue. In addition, the DODHT donor, with steric bulk arising from attachment of the *cis*-fused dioxane ring, leads to superconductors exhibiting a variety of pressure-induced resistive behaviors. An analogous compressibility that allows the appearance of the insulating, metallic, and superconducting phases can be found in β-$(BDA\text{-}TTP)_2X$ (X = $GaCl_4$ and $FeCl_4$). We therefore believe that structural modification of the π-donor skeleton to create soft donor packing motifs is a step in a new direction in achieving superconductivity and hope that derived superconductors display unconventional physical properties under applied pressures due to a high compressibility resulting from soft donor packing motifs.

Meanwhile, recent investigation of β'-$(ET)_2ICl_2$ under an extremely high pressure (8.2 GPa) by Taniguchi et al. revealed that T_c of the ET-based superconductor can reach 14.2 K.[71] The BDA-TTP and DODHT superconductors have not yet shown such a high T_c, and the reason is not clear at present. However, if π-donor systems capable of bringing about the "softness" in the crystal lattices, including BDA-TTP and DODHT, yield higher T_c superconductors, comparison of their structural and electronic aspects with those of the ET-based high-T_c superconductors will provide a guide to the construction of new high-T_c superconductors. Further pursuit of this possibility is ongoing in our laboratories.

7. Acknowledgments

We express our gratitude to a number of dedicated collaborators, whose names appear in our papers

cited below. This work was supported by grants from MEXT, especially a Grant-in-Aid for Scientific Research on Priority Areas of Molecular Conductors (No. 15073102), JSPS, and the Hyogo Science and Technology Association.

8. Supporting Information Available

Figure for the temperature dependence of resistances for the DTDH-TTP salts with BF_4^-, ReO_4^-, AsF_6^-, and SbF_6^- anions (PDF). X-ray crystallographic file for $(DTDH\text{-}TTP)_2SbF_6$ (CIF). This material is available free of charge via the Internet at http://pubs.acs.org.

9. References

(1) Ferraris, J.; Cowan, D. O.; Walatka, V., Jr.; Perlstein, J. H. *J. Am. Chem. Soc.* **1973**, *95*, 948.

(2) (a) Williams, J. M.; Ferraro, J. R.; Thorn, R. J.; Carlson, K. D.; Geiser, U.; Wang, H. H.; Kini, A. M.; Whangbo, M.-H. *Organic Superconductors (Including Fullerenes) Synthesis, Structure, Properties, and Theory*; Prentice Hall; Englewood Cliffs, NJ, 1992. (b) Saito, G. In *Organic Molecular Solids: Properties and Applications*; Jones, W., Ed.; CRC Press: Boca Raton, FL, 1997; Chapter 10. (c) Ishiguro, T.; Yamaji, K.; Saito, G. *Organic Superconductors*, 2nd ed.; Fulde, P., Ed.; Springer Series Solid-State Science 88; Springer: Berlin, 1998.

(3) (a) Otsubo, T.; Takimiya, K. *Rev. Heteroatom Chem.* **1997**, *16*, 69. (b) Papavassiliou, G. C.; Terzis, A.; Delhaes, P. In *Handbook of Organic Conductive Molecules and Polymers*; Nalwa, H. S., Ed.; J. Wiley & Sons: Chichester, 1997; Vol. 1, Chapter 3. (c) Becher, J.; Lau, J.; Mørk, P. In *Electronic Materials: The Oligomer Approach*; Müllen, K., Wegner, G., Eds.; Wiley-VCH: Weinheim, 1998; p 198. (d) Segura, J. L.; Martín, N. *Angew. Chem., Int. Ed.* **2001**, *40*, 1372 and references therein. (e) Proceedings of the Fourth International Symposium on Crystalline Organic Metals, Superconductors and Ferromagnets (ISCOM) 2001. *Synth. Met.* **2003**, *133*−*134*. (f) Proceedings of the International Conference on Science and Technology of Synthetic Metals (ICSM) 2002. *Synth. Met.* **2003**, *135*−*137*. (g) Proceedings of ISCOM 2003. *J. Phys. IV Fr.* **2004**, *114*.

(4) Bourbonnais, C.; Jérome, D. In *Advances in Synthetic Metals*—*Twenty Years of Progress in Science and Technology*; Bernier, P., Lefrant, S., Bidan, G., Eds.; Elsevier: Amsterdam, 1999; Chapter 3.

(5) (a) Kanoda, K. *Hyperfine Interact.* **1997**, *104*, 235. (b) Kanoda, K. *Physica C* **1997**, *282*−*287*, 299.

(6) For our earlier reviews, see: (a) Yamada, J. *Recent Res. Devel. Org. Chem.* **1998**, *2*, 525. (b) Yamada, J.; Nishikawa, H.; Kikuchi, K. *J. Mater. Chem.* **1999**, *9*, 617. (c) Yamada, J. *Trends Org. Chem.* **2001**, *9*, 115. (d) Yamada, J.; Nishikawa, H.; Kikuchi, K. In *TTF Chemistry*—*Fundamentals and Applications of Tetrathiafulvalene*; Yamada, J., Sugimoto, T., Eds.; Kodansha & Springer: Tokyo, 2004; Chapter 11. (e) Yamada, J. *J. Mater. Chem.* **2004**, DOI: 10.1039/b408899a.

(7) *TTF Chemistry*—*Fundamentals and Applications of Tetrathiafulvalene*; Yamada, J., Sugimoto, T., Eds.; Kodansha & Springer: Tokyo, 2004.

(8) (a) Svenstrup, N.; Becher, J. *Synthesis* **1995**, 215. (b) Simonsen, K. B.; Svenstrup, N.; Lau, J.; Simonsen, O.; Mørk, P.; Kristensen, G. J.; Becher, J. *Synthesis* **1996**, 407.

(9) (a) Otsubo, T.; Takimiya, K. *Bull. Chem. Soc. Jpn.* **2004**, *77*, 43. (b) Takimiya, K.; Otsubo, T. In *TTF Chemistry*—*Fundamentals and Applications of Tetrathiafulvalene*; Yamada, J., Sugimoto, T., Eds.; Kodansha & Springer: Tokyo, 2004; Chapter 5.

(10) (a) Yamada, J.; Amano, Y.; Takasaki, S.; Nakanishi, R.; Matsumoto, K.; Satoki, S.; Anzai, H. *J. Am. Chem. Soc.* **1995**, *117*, 1149. (b) Yamada, J.; Takasaki, S.; Kobayashi, M.; Anzai, H.; Tajima, N.; Tamura, M.; Nishio, Y.; Kajita, K. *Chem. Lett.* **1995**, 1069. (c) Yamada, J.; Satoki, S.; Mishima, S.; Akashi, N.; Takahashi, K.; Masuda, N.; Nishimoto, Y.; Takasaki, S.; Anzai, H. *J. Org. Chem.* **1996**, *61*, 3987. (d) Yamada, J.; Satoki, S.; Anzai, H.; Hagiya, K.; Tamura, M.; Nishio, Y.; Kajita, K.; Watanabe, E.; Konno, M.; Sato, T.; Nishikawa, H.; Kikuchi, K. *Chem. Commun.* **1996**, 1955. (e) Yamada, J.; Kawagishi, S.; Shinomaru, T.; Akutsu, H.; Nakatsuji, S.; Nishikawa, H.; Ikemoto, I.; Kikuchi, K. *Synth. Met.* **2001**, *120*, 787.

(11) (a) Fabre, J.-M. In *TTF Chemistry*—*Fundamentals and Applications of Tetrathiafulvalene*; Yamada, J., Sugimoto, T., Eds.; Kodansha & Springer: Tokyo, 2004; Chapter 1. (b) Papavassilious, G. C. In *TTF Chemistry*— *Fundamentals and Applications of Tetrathiafulvalene*; Yamada, J., Sugimoto, T., Eds.; Kodansha & Springer: Tokyo, 2004; Chapter 2.

(12) (a) Papavassiliou, G. C.; Mousdis, G. A.; Zameounis, J. S.; Terzis, A.; Hountas, A.; Hilti, B.; Mayer, C. W.; Pfeiffer, J. *Synth. Met.* **1988**, *27*, B379. (b) Kini, A. M.; Beno, M. A.; Son, D.; Wang, H. H.; Carlson, K. D.; Porter, L. C.; Welp, U.; Vogt, B. A.; Williams, J. M. *Solid State Commun.* **1989**, *69*, 503.

(13) Kikuchi, K.; Kikuchi, M.; Namiki, T.; Saito, K.; Ikemoto, I.; Murata, K.; Ishiguro, T.; Kobayashi, K. *Chem. Lett.* **1987**, 931.

(14) Kato, R.; Yamamoto, K.; Okano, Y.; Tajima, H.; Sawa, H. *Chem. Commun.* **1997**, 947.

(15) Yamada, J.; Mishima, S.; Anzai, H.; Tamura, M.; Nishio, Y.; Kajita, K.; Sato, T.; Nishikawa, H.; Ikemoto, I.; Kikuchi, K. *Chem. Commun.* **1996**, 2517.

(16) (a) Fabre, J. M.; Giral, L.; Dupart, E.; Coulon, C.; Manceau, J. P.; Delhaes, P. *J. Chem. Soc., Chem. Commun.* **1983**, 1477. (b) Kikuchi, K.; Yakushi, K.; Kuroda, H.; Ikemoto, I.; Kobayashi, K. *Mol. Cryst. Liq. Cryst.* **1985**, *125*, 345.

(17) (a) Yamada, J.; Nishimoto, Y.; Tanaka, S.; Nakanishi, R.; Hagiya, K.; Anzai, H. *Tetrahedron Lett.* **1995**, 36, 9509. (b) Yamada, J.; Tanaka, S.; Segawa, J.; Hamasaki, M.; Hagiya, K.; Anzai, H.; Nishikawa, H.; Ikemoto, I.; Kikuchi, K. *J. Org. Chem.* **1998**, *63*, 3952.

(18) Kotov, A. I.; Faulmann, C.; Cassoux, P.; Yagubskii, E. B. *J. Org. Chem.* **1994**, *59*, 2626.

(19) (a) Nishikawa, H.; Ishikawa, H.; Sato, T.; Kodama, T.; Ikemoto, I.; Kikuchi, K.; Tanaka, S.; Anzai, H.; Yamada, J. *J. Mater. Chem.* **1998**, *8*, 1321. (b) Yamada, J.; Akutsu, H.; Nakatsuji, S.; Nishikawa, H.; Ikemoto, I.; Kikuchi, K. *Mol. Cryst. Liq. Cryst.* **2001**, *356*, 253. (c) Kikuchi, K.; Ikeda, S.; Nishikawa, H.; Kodama, T.; Ikemoto, I.; Yamada, J. *Synth. Met.* **2001**, *120*, 901.

(20) Yamada, J.; Hamasaki, M.; Jinih, O.; Tanaka, S.; Hagiya, K.; Anzai, H. *Tetrahedron Lett.* **1997**, *38*, 3439.

(21) (a) Yamada, J.; Oka, R.; Anzai, H.; Nishikawa, H.; Ikemoto, I.; Kikuchi, K. *Tetrahedron Lett.* **1998**, *39*, 7709. (b) Yamada, J.; Oka, R.; Mangetsu, T.; Akutsu, H.; Nakatsuji, S.; Nishikawa, H.; Ikemoto, I.; Kikuchi, K. *Chem. Mater.* **2001**, *13*, 1770.

(22) Yamada, J.; Mangetsu, T.; Akutsu, H.; Nakatsuji, S.; Nishikawa, H.; Ikemoto, I.; Kikuchi, K. *Chem. Lett.* **2001**, 86.

(23) For example, see: (a) Papavassiliou, G. C.; Zambounis, J. S.; Mousdis, G. A.; Gionis, V.; Yiannopoulos, S. Y. *Mol. Cryst. Liq. Cryst.* **1988**, *156*, 269. (b) Papavassiliou, G. C.; Kakoussis, V. C.; Mousdis, G. A.; Zambounis, J. S.; Mayer, C. W. *Chem. Scr.* **1989**, *29*, 71 and references therein. (c) Singh, J. D.; Singh, H. B. *J. Chem. Soc., Perkin Trans. 1* **1992**, 2913. (a) Goldenberg, L. M.; Khodorkovsky, V. Y.; Becker, J. Y.; Lukes, P. J.; Bryce, M. R.; Petty, M. C.; Yarwood, J. *Chem. Mater.* **1994**, *6*, 1426.

(24) Engler, E. M.; Patel, V. V.; Andersen, J. R.; Schumaker, R. R.; Fukushima, A. A. *J. Am. Chem. Soc.* **1978**, *100*, 3769.

(25) Yamada, J.; Aoki, K.; Nakatsuji, S.; Nishikawa, H.; Ikemoto, I.; Kikuchi, K. *Tetrahedron Lett.* **1999**, *40*, 6635.

(26) Yamada, J.; Hayashi, R.; Akutsu, H.; Nakatsuji, S.; Nishikawa, H.; Ikemoto, I.; Kikuchi, K. *Mol. Cryst. Liq. Cryst.*, accepted for publication.

(27) Hellberg, J.; Balodis, K.; Moge, M.; Korall, P.; von Schütz, J.-U. *J. Mater. Chem.* **1997**, *7*, 31.

(28) Yamashita, Y.; Tomura, M.; Imaeda, K. *Mol. Cryst. Liq. Cryst.* **2002**, *380*, 203.

(29) Medne, R. S.; Katsens, Y. Y.; Kraupha, I. L.; Neilands, O. Y. *Khim. Geterotsikl. Soedin.* **1991**, 1317. For the I_3 salt of **30**, see: Shibaeva, R. P.; Rozenberg, L. P. Kristallografiya **1991**, *36*, 1158. Quite recently, metallic salts derived from TTF derivatives with a *cis*-fused cycloalkane have been reported, see: Suzuki, H.; Yamashita, K.; Suto, M.; Maejima, T.; Kimura, S.; Mori, H.; Nishio, Y.; Kajita, K.; Moriyama, H. *Synth. Met.* **2004**, *144*, 89 and Kimura, S.; Suzuki, H.; Maejima, T.; Suto, M.; Yamashita, K.; Ichikawa, S.; Mori, H.; Moriyama, H.; Mochida, T.; Nishio, Y.; Kajita, K. *J. Phys. IV Fr.* **2004**, *114*, 521.

(30) Kini, A. M.; Geiser, U.; Wang, H.-H.; Lykke, K. R.; Williams, J. M.; Campana, C. F. *J. Mater. Chem.* **1995**, *5*, 1647.

(31) Kobayashi, H.; Kobayashi, A.; Sasaki, Y.; Saito, G.; Inokuchi, H. *Bull. Chem. Soc. Jpn.* **1986**, *59*, 301.

(32) Yamada, J.; Tanaka, S.; Anzai, H.; Sato, T.; Nishikawa, H.; Ikemoto, I.; Kikuchi, K. *J. Mater. Chem.* **1997**, *7*, 1311.

(33) (a) Kaminskii, V. F.; Prokhorova, T. G.; Shibaeva, R. P.; Yagubskii, E. B. *Pis'ma Zh. Eksp. Teor. Fiz.* **1984**, *39*, 15. (b) Williams, J. M.; Emge, T. J.; Wang, H. H.; Beno, M. A.; Copps, P. T.; Hall, L. N.; Carlson, K. D.; Crabtree, G. W. *Inorg. Chem.* **1984**, *23*, 2558. (c) Mori, T.; Kobayashi, A.; Sasaki, Y.; Kobayashi, H.; Saito, G.; Inokuchi, H. *Chem. Lett.* **1984**, 957.

(34) For the parameters used herein for calculation of the intermolecular overlap integrals, see: Mori, T.; Kobayashi, A.; Sasaki, Y.; Kobayashi, H.; Saito, G.; Inokuchi, H. *Bull. Chem. Soc. Jpn.* **1984**, *57*, 627.

(35) Kotov, A. I.; Buravov, L. I.; Gritsenko, V. V.; Bardin, A. A.; Konovalikhin, S. V.; Dyachenko, O. A.; Yagubskii, E. B.; Van, K. V.; Mizuno, M. *Synth. Met.* **2001**, *120*, 861.

(36) Kini, A. M.; Beno, M. A.; Williams, J. M. *J. Chem. Soc., Chem. Commun.* **1987**, 335.

(37) Zambounis, J. S.; Pfeiffer, J.; Papavassiliou, G. C.; Lagouvardos, D. J.; Terzis, A.; Paptopoulou, C. P.; Delhaés, P.; Ducasse, L.; Fortune, N. A.; Murata, K. *Solid State Commun.* **1995**, *95*, 211.
(38) For another example, see: Imakubo, T.; Sawa, H.; Kato, R. *J. Chem. Soc., Chem. Commun.* **1995**, 1667.
(39) (a) Kobayashi, H.; Mori, T.; Kato, R.; Kobayashi, A.; Sasaki, Y.; Saito, G.; Inokuchi, H. *Chem. Lett.* **1983**, 581. (b) Mori, T.; Kobayashi, A.; Sasaki, Y.; Kato, R.; Kobayashi, H. *Solid State Commun.* **1985**, *53*, 627.
(40) Beno, M. A.; Geiser, U.; Kini, A. M.; Wang, H. H.; Carlson, K. D.; Miller, M. M.; Allen, T. J.; Schlueter, J. A.; Proksch, R. B.; Williams, J. M. *Synth. Met.* **1988**, *27*, A209.
(41) Coffen, D. L.; Chambers, J. Q.; Williams, D. R.; Garrett, P. E.; Canfield, N. D. *J. Am. Chem. Soc.* **1971**, *93*, 2258.
(42) Mori, T.; Inokuchi, H. *Chem. Lett.* **1992**, 1873.
(43) (a) Nishikawa, H.; Morimoto, T.; Kodama, T.; Ikemoto, I.; Kikuchi, K.; Yamada, J.; Yoshino, H.; Murata, K. *J. Am. Chem. Soc.* **2002**, *124*, 730. (b) Nishikawa, H.; Morimoto, T.; Kodama, T.; Ikemoto, I.; Kikuchi, K.; Yamada, J.; Yoshino, H.; Murata, K. *Synth. Met.* **2003**, *133*−*134*, 193. (c) Nishikawa, H.; Machida, A.; Morimoto, T.; Kikuchi, K.; Kodama, T.; Ikemoto, I.; Yamada, J.; Yoshino, H.; Murta, K. *Chem. Commun.* **2003**, 494. (d) Nishikawa, H.; Sato, Y.; Kodama, T.; Kikuchi, K.; Ikemoto, I.; Yamada, J. *J. Phys. IV Fr.* **2004**, *114*, 565.
(44) Kikuchi, K.; Nishikawa, H.; Sato, T.; Isaka, T.; Kodama, T.; Ikemoto, I.; Anzai, H.; Yamada, J. *Synth. Met.* **1999**, *102*, 1624.
(45) (a) Kobayashi, H.; Kato, R.; Kobayashi, A.; Nishio, Y.; Kajita, K.; Sasaki, W. *Chem. Lett.* **1986**, 789. (b) Kobayashi, H.; Kato, R.; Kobayashi, A.; Nishio, Y.; Kajita, K.; Sasaki, W. *Chem. Lett.* **1986**, 833.
(46) (a) Mori, H.; Tanaka, S.; Mori, T. *Phys. Rev. B* **1988**, *57*, 12023. (b) Mori, T.; Mori, H.; Tanaka, S. *Bull. Chem. Soc. Jpn.* **1999**, *72*, 179.
(47) Mori, T. *Bull. Chem. Soc. Jpn.* **1998**, *71*, 2509.
(48) For other superconducting hydrates, see: (a) Mori, T.; Inokuchi, H. *Solid State Commun.* **1987**, *64*, 335. (b) Mori, H.; Hirabayashi, I.; Tanaka, S.; Mori, T.; Inokuchi, H. *Solid State Commun.* **1990**, *76*, 35. (c) Mori, H.; Hirabayashi, I.; Tanaka, S.; Mori, T.; Maruyama, Y.; Inokuchi, H. *Solid State Commun.* **1991**, *80*, 411. (d) Kahlich, S.; Schweitzer, D.; Heinen, I.; Lan, S. E.; Nuber, B.; Keller, H. J.; Winzer, K.; Helberg, H. W. *Solid State Commun.* **1991**, *80*, 191. (e) Mori, T.; Kato, K.; Maruyama, Y.; Inokuchi, H.; Mori, H.; Hirabayashi, I.; Tanaka, S. *Solid State Commun.* **1992**, *82*, 177.
(49) Setifi, F.; Ouahab, L.; Golhen, S.; Hernandez, O.; Miyazaki, A.; Enoki, T.; Toita, T.; Yamada, J.; Nishikawa, H.; Lapinski, A.; Swietlik, R. *Inorg. Chem.* **2002**, *41*, 3761.
(50) Schumaker, R. R.; Engler, E. M. *J. Am. Chem. Soc.* **1977**, *99*, 5519.
(51) Misaki, Y. In *TTF Chemistry—Fundamentals and Applications of Tetrathiafulvalene*; Yamada, J., Sugimoto, T., Eds.; Kodansha & Springer: Tokyo, 2004; Chapter 10.
(52) Misaki, Y.; Higuchi, N.; Fujiwara, H.; Yamabe, T.; Mori, T.; Mori, H.; Tanaka, S. *Angew. Chem., Int. Ed. Engl.* **1995**, *34*, 1222. For the revised stoichiometry of this superconductor, see: Misaki, Y.; Higuchi, N.; Ohta, T.; Fujiwara, H.; Yamabe, T.; Mori, T.; Mori, H.; Tanaka, S. *Mol. Cryst. Liq. Cryst.* **1996**, *284*, 27.
(53) Yamada, J.; Watanabe, M.; Akutsu, H.; Nakatsuji, S.; Nishikawa, H.; Ikemoto, I.; Kikuchi, K. Unpublished results.
(54) Setifi, F.; Ouahab, L.; Golhen, S.; Miyazaki, A.; Enoki, T.; Yamada, J. *C. R. Chim.* **2003**, *6*, 309.
(55) Urayama, H.; Yamachi, H.; Saito, G.; Sato, S.; Kawamoto, A.; Tanaka, J.; Mori, T.; Maruyama, Y.; Inokuchi, H. *Chem. Lett.* **1988**, 463.
(56) Yamada, J.; Akashi, N.; Anzai, H.; Tamura, M.; Nishio, Y.; Kajita, K. *Mol. Cryst. Liq. Cryst.* **1997**, *296*, 53.
(57) (a) Yamada, J.; Watanabe, M.; Anzai, H.; Nishikawa, H.; Ikemoto, I.; Kikuchi, K. *Angew. Chem., Int. Ed. Engl.* **1999**, *38*, 810. (b) Yamada, J.; Watanabe, M.; Akutsu, H.; Nakatsuji, S.; Nishikawa, H.; Ikemoto, I.; Kikuchi, K. *J. Am. Chem. Soc.* **2001**, *123*, 4174. (c) Nishikawa, H.; Isaka, T.; Kodama, T.; Ikemoto, I.; Kikuchi, K.; Yamada, J.; Misaki, Y. *Synth. Met.* **2001**, *120*, 903. (d) Yamada, J.; Watanabe, M.; Toita, T.; Akutsu, H.; Nakatsuji, S.; Nishikawa, H.; Ikemoto, I.; Kikuchi, K. *Chem. Commun.* **2002**, 1118. (e) Yamada, J.; Toita, T.; Akutsu, H.; Nakatsuji, S.; Nishikawa, H.; Ikemoto, I.; Kikuchi, K. *Synth. Met.* **2003**, *135*−*136*, 539.
(58) Yamada, J. *J. Phys. IV Fr.* **2004**, *114*, 439.
(59) Kikuchi, K.; Nishikawa, H.; Ikemoto, I.; Toita, T.; Akutsu, H.; Nakatsuji, S.; Yamada, J. *J. Solid State Commun.* **2002**, *168*, 503.
(60) Setifi, F.; Golhen, S.; Ouahab, L.; Miyazaki, A.; Okabe, K.; Enoki, T.; Toita, T.; Yamada, J. *Inorg. Chem.* **2002**, *41*, 3786.
(61) (a) Shibaeva, R.; Khasanov, S.; Zorina, L.; Simonov, S.; Shevyakova, I.; Kushch, L.; Buravov, L.; Yagubskii, E.; Baudron, S.; Méziére, C.; Batail, P.; Canadell, E.; Yamada, J. *J. Phys. IV Fr.* **2004**, *114*, 481. (b) Shevyakova, I.; Buravov, L.; Tkacheva, V.; Zorina, L.; Khasanov, S.; Simonov, S.; Yamada, J.; Canadell, E.; Shibaeva, R.; Yagubskii, E. *Adv. Funct. Mater.* **2004**, *14*, 660.
(62) Shimojo, Y.; Ishiguro, T.; Toita, T.; Yamada, J. *J. Phys. Soc. Jpn.* **2002**, *71*, 717.
(63) Choi, E. S.; Jobilong, E.; Wade, A.; Goetz, E.; Brooks, J. S.; Yamada, J.; Mizutani, T.; Kinoshita, T.; Tokumoto, M. *Phys. Rev. B* **2003**, *67*, 174511.
(64) Oshima, K.; Mori, T.; Inokuchi, H.; Urayama, H.; Yamachi, H.; Saito, G. *Phys. Rev. B* **1988**, *38*, 938.
(65) (a) Yamada, J.; Toita, T.; Akutsu, H.; Nakatsuji, S.; Nishikawa, H.; Ikemoto, I.; Kikuchi, K.; Choi, E. S.; Graf, D.; Brooks, J. S. *Chem. Commun.* **2003**, 2230. (b) Choi, E. S.; Graf, D.; Brooks, J. S.; Yamada, J.; Tokumoto, M. *J. Phys. IV Fr.* **2004**, *114*, 297. (c) Choi, E. S.; Graf, D.; Brooks, J. S.; Yamada, J.; Akutsu, H.; Kikuchi, K.; Tokumoto, M. *Phys. Rev. B* **2004**, *70*, 024517.
(66) Yamada, J.; Toita, T.; Akutsu, H.; Nakatsuji, S.; Nishikawa, H.; Ikemoto, I.; Kikuchi, K. *Chem. Commun.* **2001**, 2538.
(67) Tanaka, H.; Adachi, T.; Ojima, E.; Fujiwara, H.; Kato, K.; Kobayashi, H.; Kobayashi, A.; Cassoux, P. *J. Am. Chem. Soc.* **1999**, *121*, 11243.
(68) Yamada, J.; Watanabe, M.; Toita, T.; Akutsu, H.; Nakatsuji, S.; Nishikawa, H.; Ikemoto, I.; Kikuchi, K. *Synth. Met.* **2003**, *133*−*134*, 189.
(69) Jérome, D.; Mazaud, A.; Ribault, M.; Bechgaard, K. *J. Phys. Lett.* **1980**, *41*, L-95.
(70) For new TCF donors which have recently been reported to give organic superconductors, see: (a) Takimiya, K.; Kataoka, Y.; Aso, Y.; Otsubo, T.; Fukuoka, H.; Yamanaka, S. *Angew. Chem., Int. Ed.* **2001**, *40*, 1122. (b) Imakubo, T.; Tajima, N.; Tamura, M.; Kato, R.; Nishio, Y.; Kajita, K. *J. Mater. Chem.* **2002**, *12*, 159. (c) Kodani, M.; Takamori, A.; Takimiya, K.; Aso, Y.; Otsubo, T. *J. Solid State Chem.* **2002**, *168*, 582. (d) Takimiya, K.; Takamori, A.; Aso, Y.; Otsubo, T.; Kawamoto, T.; Mori, T. *Chem. Mater.* **2003**, *15*, 1225. (e) Takimiya, K.; Kodani, M.; Kataoka, Y.; Aso, Y.; Otsubo, T.; Kawamoto, T.; Mori, T. *Chem. Mater.* **2003**, *15*, 3250.
(71) Taniguchi, H.; Miyashita, M.; Uchiyama, K.; Satoh, K.; Môri, N.; Okamoto, H.; Miyagawa, K.; Kanoda, K.; Hedo, M.; Uwatoko, Y. *J. Phys. Soc. Jpn.* **2003**, *72*, 468.

CR0306687